Amplitude analysis of the K^-K^+ system produced in the reactions $\pi^-p\to K^-K^+n$ and $\pi^+n\to K^-K^+p$ at 6 GeV/c

D. Cohen,* D. S. Ayres, R. Diebold, S. L. Kramer, A. J. Pawlicki,† and A. B. Wicklund
Argonne National Laboratory, Argonne, Illinois 60439
(Received 28 August 1978; revised manuscript received 14 July 1980)

We have carried out an amplitude analysis of the K^-K^+ system produced in the reactions $\pi^-p\to K^-K^+n$ and $\pi^+n\to K^-K^+p$ using data from a high-statistics experiment performed with the Argonne effective-mass spectrometer. Combining the results from the two reactions allows us to analyze the $\bar{K}K$ production amplitudes in terms of their isospin-zero and -one components. We use phenomenological arguments based on t dependence and on the expected properties of the P and D waves to resolve ambiguities. Our favored solution exhibits an enhancement around 1300 MeV in the isospin-zero S wave produced by π exchange. In this solution the Argand plot for the $\pi\pi\to\bar{K}K$ S wave changes rapidly above 1300 MeV, consistent with a resonance at 1425 ± 15 MeV with width 160 ± 30 MeV. We show that our solution is consistent with the features of neutral and charged $\bar{K}K$ systems found in other experiments.

I. INTRODUCTION

We have carried out an amplitude analysis of the K^-K^+ system produced in the reactions

$$\pi^-p\to K^-K^+n \tag{1}$$

and

$$\pi^+n\to K^-K^+p \tag{2}$$

at 6 GeV/c. The data were obtained in a high-statistics experiment,[1] using the Argonne effective-mass spectrometer, which yielded 110 000 events from reaction (1) and 50 000 events from reaction (2).

The quantum numbers of the K^-K^+ system are restricted to the series $J^{PC}=0^{++}$ [$S^*(980)$, $\epsilon(\sim1300)$, $\delta(980)$], 1^{--} (ω,ϕ,ρ), 2^{++} (f,f',A_2), 3^{--} [$\omega(1675)$, g], etc., where we have shown explicitly the states that are potentially important in our study. The isotopic spin I of the K^-K^+ system can be either zero or one, with its G parity given by $(-1)^{I+J}$.

Our motivation for studying $\bar{K}K$ production using both reactions (1) and (2) arises from the observation[2] that if we define A_0 and A_1 to be the amplitudes for producing an $I=0$ and $I=1$ K^-K^+ system, respectively, in reaction (1), then the total amplitude for this reaction is $A(\pi^-p\to K^-K^+n)=A_0+A_1$, while the amplitude for the reaction $\pi^-p\to\bar{K}^0K^0n$ is A_0-A_1. By charge independence the amplitude for reaction (2) is the same as for the latter reaction, namely $A(\pi^+n\to K^-K^+p)=A_0-A_1$. Using the standard symbols for the meson states to represent the various amplitudes, we can symbolically write the differential cross sections for reactions (1) and (2) as

$$\frac{d^2\sigma^{\mp}}{dt\,dM}=|S^*+\epsilon\pm\delta^0|^2+|\phi\pm\rho^0|^2+|f+f'\pm A_2^0|^2+\cdots,$$

where the superscripts $-$ and $+$ refer to reactions (1) and (2), respectively, M is the K^-K^+ effective mass, and t is the four-momentum transfer to the recoil nucleon. Similar relations involving interference between different spin states hold for the various K^-K^+ decay angular-distribution moments. Thus, comparison of $\bar{K}K$ production off p and n targets helps to separate the produced $\bar{K}K$ system into its $I=0$ and $I=1$ components.

One of the major thrusts of this paper is to arrive at a better understanding of the $J^{PC}=0^{++}$ S wave in $\bar{K}K$, partly because recent analyses[1,3–7] have disagreed sharply on the nature of this system, but primarily because the S-wave states are of central importance to quark-model spectroscopy. Morgan,[8] for example, has classified the scalar mesons into a nonideally mixed nonet with a mixing angle of ~68°. Taking the states to be the $\delta(980)$, $S^*(980)$, $\kappa(1250)$, and the $\epsilon(1300)$, he was able to obtain a self-consistent set of masses and coupling constants. The large deviation from ideal mixing and the approximate mass degeneracy of S^* and δ are not explained in the Morgan scheme. Furthermore, possible additional 0^{++} states, such as the enhancement in $\bar{K}K$ near 1300 MeV discussed below and the $K\pi$ S-wave resonance near 1500 MeV discussed by Estabrooks *et al.*,[9] are not readily accommodated in Morgan's classification. Jaffe has proposed an alternative scheme involving two 0^{++} nonets.[10] In this model the lower-mass states $\epsilon(800)$, $\kappa(900)$, $S^*(980)$, and $\delta(980)$ would comprise a four-quark nonet, while the states in the conventional $Q\bar{Q}$ nonet would lie in the 1200–1600 MeV mass region. This scheme can accommodate possible new states as QQ systems. However, there is no direct evidence for a $\kappa(900)$ state, and its existence requires a rather unconventional interpre-

tation of the $K\pi$ phase shifts.[11] In any case, a more detailed understanding of the scalar-meson spectrum above 1 GeV is needed in order to distinguish between these models.

Two recent experiments have been carried out on the reaction

$$\pi^- p \to K_S K_S n, \tag{3}$$

each yielding about 6000 events. Cason *et al.*[3] used the Argonne streamer chamber to study the reaction at 6 and 7 GeV/c, while Wetzel *et al.*[4] used optical spark chambers at 9 GeV/c. Both experiments observed a sharp negative excursion in the $\langle Y_2^0 \rangle$ moment of the $K_S K_S$ decay angular distribution near a mass of 1200 MeV; since the $K_S K_S$ system can only have even partial waves, i.e., $J^{PC} = 0^{++}, 2^{++}, \ldots$, this excursion was ascribed to SD interference. The authors of each experiment performed an amplitude analysis of their own data, in each case finding substantial S wave in the 1200–1400 MeV mass region in addition to the D-wave peak coming from f-meson production. Although the experimental results of the two groups are in excellent agreement within the statistical uncertainties, the S-wave amplitude found by Wetzel *et al.* appears quite flat in this mass region, linking up smoothly to the lower-mass S^* region, while the amplitude found by Cason *et al.* shows an enhancement in the 1300-MeV region. Even though their analysis gave two solutions and, with only one reaction under study, could not directly observe isospin effects, Cason *et al.* ascribed this enhancement to a relatively narrow ($\Gamma = 80$ MeV) resonance with $I = 1$. With our better statistics we have indeed confirmed the existence of an enhancement, but find that the effect occurs in the $I = 0$ S wave and is quite broad, with no obvious resonant phase variation.[6]

Martin *et al.*[5] have carried out a study of the reaction

$$\pi^- p \to K^- K_S^0 p \tag{4}$$

at 10 GeV/c. This reaction is simpler than those with K^-K^+ and $K_S K_S$ in that only $I = 1$ $\bar{K}K$ states are allowed, but more complicated in that both $I = 0$ and $I = 1$ exchanges are allowed. These authors observed a small enhancement in the 1300-MeV region which could be either S wave or P wave depending on which of two ambiguous solutions is taken. By comparing the threshold behavior of the two solutions, the authors argued for the S-wave-dominated solution and thereby claimed evidence for an $I = 1$ S-wave structure near 1300 MeV.

We have previously presented discussions[1,6,7] of the K^-K^+ amplitudes based on preliminary amplitude analysis of our data for reactions (1) and (2). In this paper we present the details and results of our final analysis, including the results of all eight mathematically allowed solutions. All but one of these solutions give amplitudes with unexpectedly rapid variations in magnitude and phase, as well as t dependences at variance with those expected on phenomenological grounds. The one remaining solution shows that the enhancement near 1300 MeV is a broad effect in the $I = 0$ S wave, the $I = 1$ S wave being small and featureless. This solution is consistent with the $I = 0$ S wave being produced mainly by one-pion exchange, as might be expected, and also gives small, but significant, P-wave amplitudes, consistent with simple extrapolations of the ρ^0 and ω Breit-Wigner tails.

The experimental method is outlined in Sec. II. The method and results of our amplitude analysis are presented in Sec. III, while Sec. IV investigates the character of the mathematically allowed solutions and makes physical arguments for the favored solution. Section V compares our results with those from the other $\bar{K}K$ experiments, and Sec. VI presents our analysis of the $I = 0$ S wave based on coupled-channel unitarity constraints. Section VII summarizes our results and conclusions.

II. EXPERIMENTAL METHOD

The data for reactions (1) and (2) were obtained using the Argonne effective-mass spectrometer and a 6-GeV/c unseparated beam. The apparatus is shown in Fig. 1. The forward K^- and K^+ were measured with the sets of magnetostrictive-readout spark chambers, $K1$ through $K5$; the spectrometer magnet had an $\int B\,dl$ of 11.4 kG m. The threshold Čerenkov counter C_τ vetoed reactions with fast pions. No attempt was made to measure the recoil particles. A detailed description of the apparatus, the trigger requirements, and the event selection criteria has been presented in Ref. 1.

All events passing the selection criteria were analyzed assuming that a particle-antiparticle pair was produced along with a recoil nucleon, i.e., that the reactions were of the type $\pi^- p \to A^- A^+ n$ and $\pi^+ n \to A^- A^+ p$. The square of the mass of A, M_A^2, was then calculated, and these M_A^2 distributions were used to define the K^-K^+N signal region and to determine the background within this region. This background consisted mainly of events of the type $\pi^\pm N \to \pi^-\pi^+ X$ where both pions failed to count in C_τ, and events of the type $\pi^\pm N \to K^-K^+(N\pi)$. The former were studied using data recorded without the C_τ veto requirement in the trigger.

The data were binned in M and t, and the moments of the K^-K^+ angular distribution were cal-

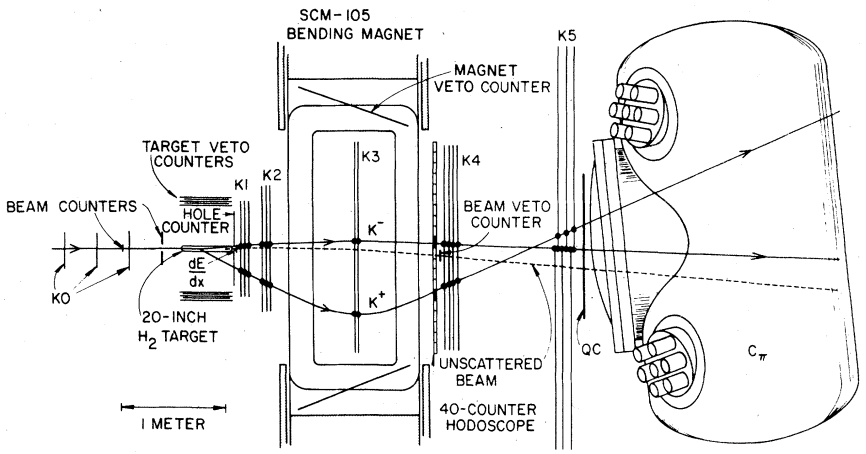

FIG. 1. Plan view of the Argonne effective-mass spectrometer. $K0$ through $K5$ are sets of magnetostrictive-readout wire spark chambers. C_π is a Freon-filled threshold Čerenkov counter.

culated for each bin in the t-channel (Jackson) frame. The moments were calculated using the maximum-likelihood method described previously,[1,12] which included the effects of spectrometer acceptance along with other experimental losses. The normalized spherical harmonic moments $\langle Y_l^m \rangle$ were defined by the relation

$$\frac{d^4\sigma}{dt\,dM\,d\Omega} = \sum_{l=0}^{l_{\max}} \sum_{m=-l}^{l} \langle Y_l^m \rangle \,\mathrm{Re}\, Y_l^m(\Omega) \frac{d^2\sigma}{dt\,dM}, \quad (5)$$

where $\Omega = (\cos\theta, \phi)$ and θ, ϕ are the angles defining the K^- direction in the t-channel frame. The moments were corrected for backgrounds coming from non-K^-K^+N final states, and have been presented in Ref. 1; tables are also available from the authors.

The overall normalization uncertainty in this experiment is estimated[1] to be $\lesssim 10\%$. The systematic uncertainties inherent in the comparison of reactions (1) and (2) are $\lesssim 5\%$.[1,12]

III. AMPLITUDE ANALYSIS

The moments of the $\bar{K}K$ decay angular distribution can be expressed as linear combinations of bilinear products of the production amplitudes[13,14] $L_{\lambda\pm}$, where $L_{\lambda\pm}$ is the amplitude for production of a $\bar{K}K$ system of spin L and helicity λ by natural (+) or unnatural (−) parity exchange. Our normalization is such that

$$\frac{d^2\sigma}{dt\,dm} = \sum_{L,\lambda} |L_{\lambda+}|^2 + |L_{\lambda-}|^2 . \quad (6)$$

The expressions for the $\langle Y_l^m \rangle$ moments up through $l=7$ in terms of the production amplitudes are given in Ref. 1. For now we restrict ourselves to the region $M < 1600$ MeV and $t_{\min} < |t| < 0.08$ GeV^2; we discuss extensions of the analysis to larger t in Secs. IV and V. For the M and t region under consideration the relative insignificance of moments[1] with $l > 4$ leads us to ignore production amplitudes with spin $L \geq 3$. In addition, the moments with $m = 3$ and 4 are consistent with zero, and we therefore ignore amplitudes with $\lambda \geq 2$. The remaining $\bar{K}K$ production amplitudes in reactions (1) and (2) are S_0, P_0, P_+, P_-, D_0, D_+, and D_-, where we have shortened the notation to $L_0 \equiv L_{0-}$ and $L_\pm \equiv L_{1\pm}$. There are, in fact, two possible amplitudes for each set of quantum numbers L and λ, one being helicity flip (f) and the other nonflip (nf) at the nucleon vertex. We are thus left with the problem of determining 14 complex amplitudes from the 12 moments with $l \leq 4$, $m \leq 2$.

To simplify the analysis, we first formed linear combinations of the $\langle Y_l^m \rangle$ moments that more clearly display the underlying amplitude structure. These combinations, labeled $\langle Q_i \rangle$ as in Ref. 1, are defined in Table I, and their decomposition in terms of bilinear products of amplitudes is given in Table II. These $\langle Q_i \rangle$ moments for reactions (1) and (2) are shown in Figs. 2 and 3, respectively. We have displayed only those $\langle Q_i \rangle$ moments corresponding to $\langle Y_l^0 \rangle$ and $\langle Y_l^1 \rangle$ terms. We have shown in Ref. 1 that the $\langle Y_l^2 \rangle$ moments are all consistent with zero for the range $|t| < 0.08$ GeV^2. These $\langle Y_l^2 \rangle$ moments are proportional to the differences $|L_-|^2 - |L_+|^2$, as explained in Ref. 1.

Physically the important amplitudes in our analysis turn out to be S_0, P_0, and D_0, the $L_\pm$ being relatively small. The possible t-channel exchanges can be labeled according to their quantum numbers as π and B (nucleon-helicity nonflip) and A_1 and Z (nucleon-helicity flip), where π and A_1 (B and Z) produce $\bar{K}K$ states having $I+J$ even (odd). At small t there is ample

TABLE I. Definition of the $\langle Q_i \rangle$ moments.

$$\langle Q_1 \rangle = \langle Y_0^0 \rangle - 1.167 \langle Y_4^0 \rangle$$
$$\langle Q_2 \rangle = 1.167 \langle Y_4^0 \rangle$$
$$\langle Q_3 \rangle = 0.500 \langle Y_2^0 \rangle - 0.373 \langle Y_4^0 \rangle$$
$$\langle Q_4 \rangle = 0.569 \langle Y_3^0 \rangle$$
$$\langle Q_5 \rangle = 0.500 \langle Y_1^0 \rangle - 0.509 \langle Y_3^0 \rangle$$
$$\langle Q_6 \rangle = 0.708 \langle Y_1^1 \rangle - 0.662 \langle Y_3^1 \rangle$$
$$\langle Q_7 \rangle = 0.912 \langle Y_2^1 \rangle - 0.372 \langle Y_4^1 \rangle$$
$$\langle Q_8 \rangle = 0.854 \langle Y_3^1 \rangle$$
$$\langle Q_9 \rangle = 0.904 \langle Y_4^1 \rangle$$

evidence that absorbed one-pion exchange (OPEA) is the dominant mechanism. Consequently, we have reduced the number of unknowns by ignoring the A_1 and Z exchange amplitudes, on the grounds that these can contribute only quadratically to the moments, which have the structure $|L^{nf}|^2 + |L^f|^2$. Similar assumptions have been made in analyses of reaction (3).[3,4]

Certainly the basic features of the moments are compatible with OPEA dominance. First, the $\langle Q_i \rangle$ moments in Figs. 2 and 3 show that S_0, P_0, and D_0 are dominant amplitudes, while P_- and D_- show up only in the small interference terms L_-L_0. Second, the vanishing of the $\langle Y_l^2 \rangle$ moments, noted above, follows naturally from OPEA; in the t channel, the $L_\pm$ amplitudes both arise from the pion-exchange absorptive cut, with the result that $|L_-|^2 - |L_+|^2 \approx 0$.[12] Both of these features have been observed in the OPEA-dominated reaction $\pi^- p \to \pi^- \pi^+ n$[12-15] In addition, the $\langle Q_i \rangle$ moments of Figs. 2 and 3 exhibit the overall symmetries expected of one-pion exchange. The

TABLE II. The moments $\sigma\langle Q_i \rangle \equiv \sqrt{4\pi}\,(d^2\sigma/dt\,dM)\langle Q_i \rangle$ in terms of the $\bar{K}K$ production amplitudes L_0, L_-, and L_+. In these expressions we use the convention that $AB \equiv \mathrm{Re}(AB^*)$ with a summation over nucleon-helicity indices implied, i.e., $AB \equiv \mathrm{Re}(A^f B^{f*}) + \mathrm{Re}(A^{nf} B^{nf*})$. Also $A^2 \equiv |A|^2 = |A^f|^2 + |A^{nf}|^2$.

$$\sigma\langle Q_1 \rangle = S_0^2 + P_0^2 + P_-^2 + P_+^2 + 1.667(D_-^2 + D_+^2)$$
$$\sigma\langle Q_2 \rangle = D_0^2 - 0.667(D_-^2 + D_+^2)$$
$$\sigma\langle Q_3 \rangle = S_0 D_0 + 0.447 P_0^2 - 0.224(P_-^2 + P_+^2) + 0.372(D_-^2 + D_+^2)$$
$$\sigma\langle Q_4 \rangle = P_0 D_0 - 0.557(P_- D_- + P_+ D_+)$$
$$\sigma\langle Q_5 \rangle = S_0 P_0 + 1.291(P_- D_- + P_+ D_+)$$
$$\sigma\langle Q_6 \rangle = S_0 P_- - 1.119 P_- D_0$$
$$\sigma\langle Q_7 \rangle = P_0 P_- + 1.290 S_0 D_-$$
$$\sigma\langle Q_8 \rangle = P_0 D_- + 0.866 P_- D_0$$
$$\sigma\langle Q_9 \rangle = D_0 D_-$$

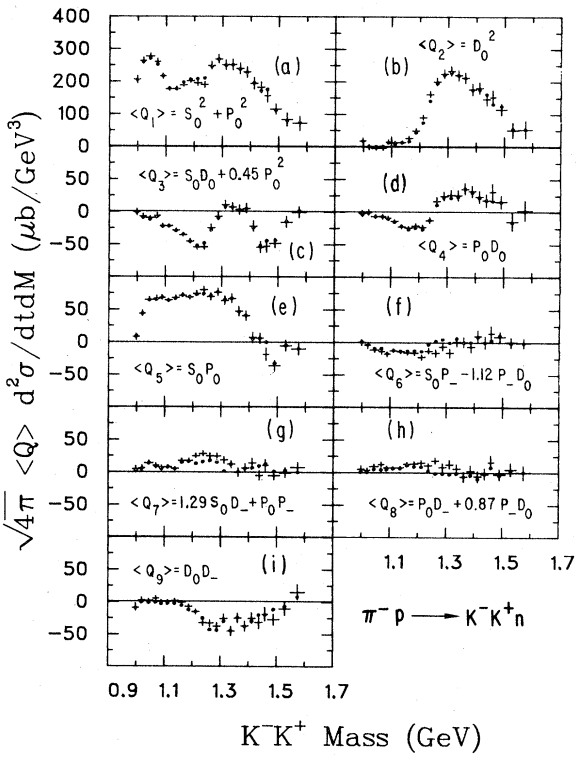

FIG. 2. $\langle Q_i \rangle$ moments for $\pi^- p \to K^- K^+ n$ averaged over the region $|t| < 0.08$ GeV^2. The dots are the result of the fit discussed in the text. The dominant amplitude contributions to the large moments are indicated; see Tables I and II for details.

SD interference terms are similar in reactions (1) and (2), while the *SP* and *PD* interferences are approximately mirror symmetric. The symmetry patterns suggest that the *S* and *D* states have a common isospin which is opposite to that of the *P* state; this is trivially explained by the fact that pion exchange can produce only $I = 0$ *S* and *D* waves and $I = 1$ *P* waves. Deviations from mirror symmetry can be explained by the *B*-exchange amplitudes, which have opposite $\bar{K}K$ isospin.

The assumption of OPEA dominance not only constrains the nucleon-helicity structure, but also suggests a parametrization of the t dependences of the amplitudes. This is potentially important in that our data are averaged over a coarse t interval, $t_{min} < |t| < 0.08$ GeV^2; the different t dependences expected for L_0 and L_- can affect the apparent coherence of these amplitudes as seen in the L_-L_0 interference terms. We have specified the form of the t-channel amplitudes as follows[12]:

$$S_0^{nf} = A_S \frac{\sqrt{-t}}{\mu^2 - t} \exp[B_{S_0}(t - \mu^2)], \quad S_0^f = 0, \qquad (7a)$$

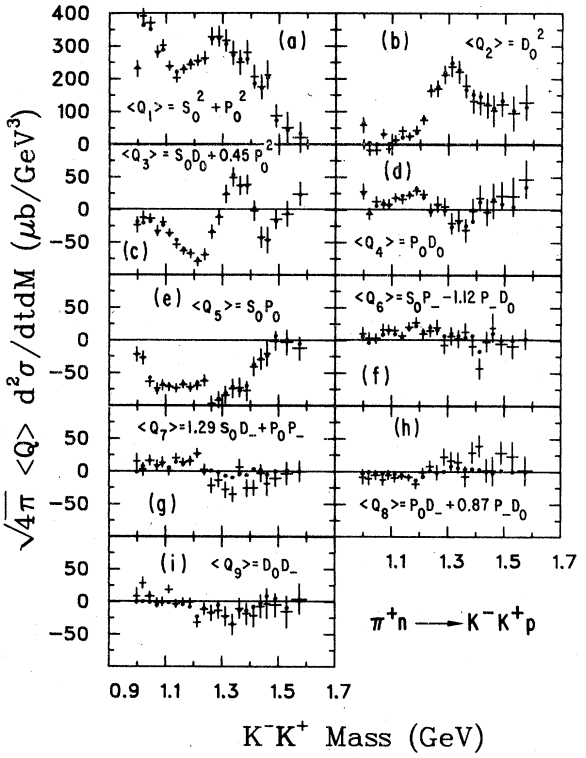

FIG. 3. $\langle Q_i\rangle$ moments for $\pi^+n \to K^-K^+p$ averaged over the region $|t| < 0.08$ GeV^2. The dots are the result of the fit discussed in the text. The dominant amplitude contributions to the large moments are indicated; see Tables I and II for details.

$$P_0^{nf} = A_{P_0}\frac{\sqrt{-t}}{\mu^2 - t}\exp[B_{P_0}(t-\mu^2)],\quad P_0^f = 0\ , \tag{7b}$$

$$D_0^{nf} = A_{D_0}\frac{\sqrt{-t}}{\mu^2 - t}\exp[B_{D_0}(t-\mu^2)],\quad D_0^f = 0\ , \tag{7c}$$

$$P_-^{nf} = A_{P_-}\left(\frac{t'}{t}\right)^{1/2}\exp(B_{P_-}t' + C_{P_-}t'^2), \tag{7d}$$

$$P_-^f = \left(\frac{t_{min}}{t'}\right)^{1/2}P_-^{nf},$$

$$D_-^{nf} = A_{D_-}\left(\frac{t'}{t}\right)^{1/2}\exp(B_{D_-}t')\quad D_-^f = \left(\frac{t_{min}}{t'}\right)^{1/2}D_-^{nf}, \tag{7e}$$

$$|P_+|^2 = |P_-|^2 = |P_-^{nf}|^2 + |P_-^f|^2\ , \tag{7f}$$

$$|D_+|^2 = |D_-|^2 = |D_-^{nf}|^2 + |D_-^f|^2\ . \tag{7g}$$

In the above $t' = t - t_{min}$ and μ denotes the pion mass. It is further assumed that P_- and P_0 are relatively real, as are D_- and D_0. The slope parameters (B_{S_0}, B_{P_0}, etc.) were taken from studies[12,14] of dipion production, and their values are listed in Table III. Reasonable variations of these parameters have a negligible effect on the determination of the dominant S_0, P_0, and D_0 terms.

The most problematic constraint in our analysis is that the A_1- and Z-exchange amplitudes, S_0^f, P_0^f, and D_0^f, are chosen to be zero. As discussed below, this constraint leads to eight discrete solutions, only one of which exhibits the expected OPEA features. Thus, the constraint may be regarded as a first approximation which is useful for resolving ambiguities. Having chosen the preferred solution, one can then always introduce nonzero values for the L_0^f waves according to a model prescription, and redetermine the L_0^{nf} waves by fixing the $\langle Q_i\rangle$ moment combinations. Martin and Ozmutlu[16] have carried out this type of analysis with our data; they find that the OPEA-dominated L_0^{nf} waves in our preferred solution are quite stable against reasonable variations in the A_1- and Z-exchange L_0^f amplitudes. We discuss their analysis further in Sec. V.

Using the OPEA constraints discussed above, we have fitted the nine $\langle Q_i\rangle$ moments in each K^-K^+ mass bin, to determine seven parameters per bin, namely the magnitudes of the independent amplitudes (S_0, P_0, D_0, P_-^{nf}, and D_-^{nf}) and the phase differences $\phi_S - \phi_D$ and $\phi_P - \phi_D$. This analysis was performed separately for reactions (1) and (2). Using the method of Barrelet zeros,[17] four sets of mathematically allowed solutions were found for each reaction; these consist of two solutions for the magnitudes of the amplitudes, each of which has two solutions for the phases. The results of the fits are shown in Figs. 2 and 3; all solutions for a given reaction gave essentially the same fit to the moments. To first order, the first five moments determine the magnitudes of the three $m = 0$ amplitudes and the two phase differences, while the remaining four moments fix the two $m = 1$ amplitudes. The assumed parametrization of the amplitudes clearly provides a good description of the experimentally measured moments.

Figure 4 shows the intensities of S_0, P_0, and D_0 for reaction (2) for $|t| < 0.08$ GeV^2. The two sets of solutions for $|S_0|^2$ and $|P_0|^2$ differ only

TABLE III. Parameters used for t dependence of the amplitudes.

B_{S_0}	3.0 GeV^{-2}
B_{P_0}	2.9 GeV^{-2}
B_{D_0}	3.7 GeV^{-2}
B_{P_-}	6.7 GeV^{-2}
C_{P_-}	4.5 GeV^{-4}
B_{D_-}	3.4 GeV^{-2}

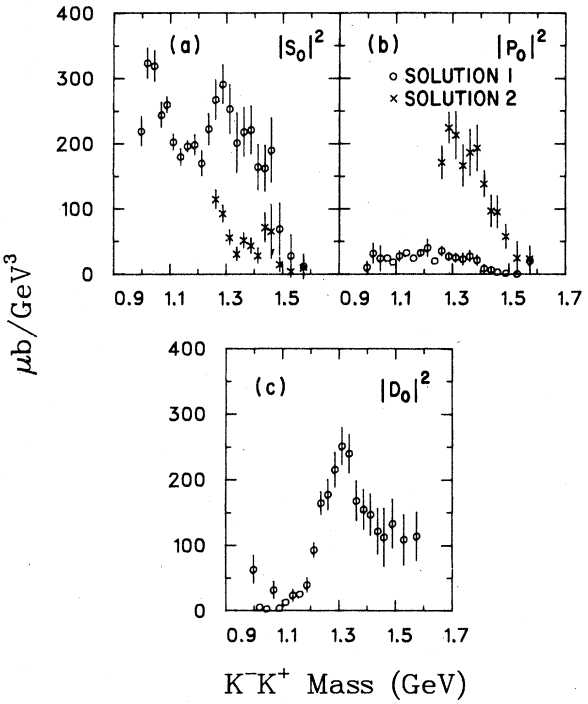

FIG. 4. S_0, P_0, and D_0 intensities for $\pi^+ n \to K^- K^+ p$ for $|t| < 0.08$ GeV^2. The two sets of solutions for S_0 and P_0 differ for $M_{\overline{K}K} > 1.2$ GeV.

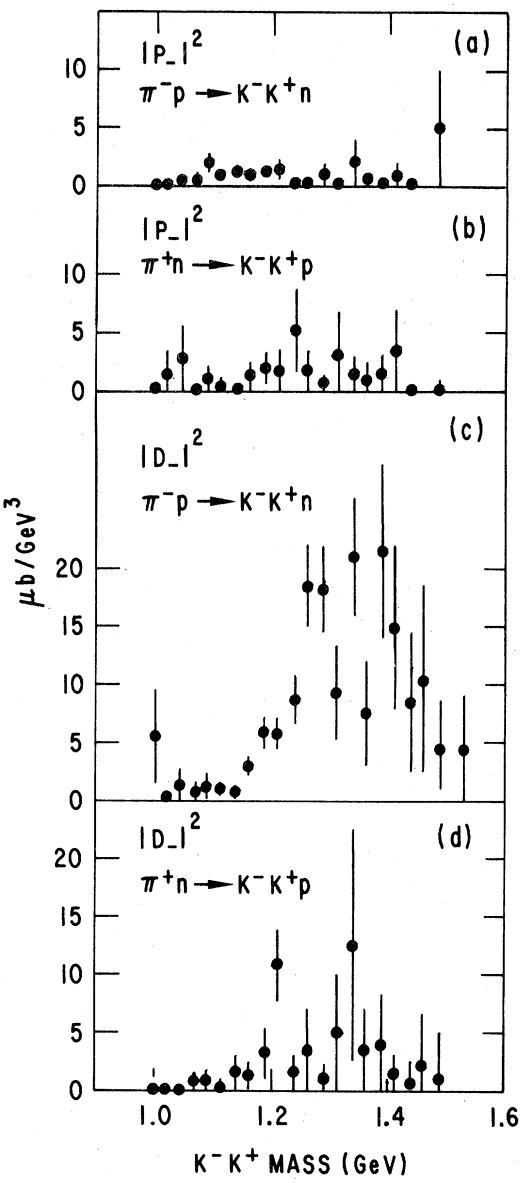

FIG. 5. $|P_-|^2 = |P_-^f|^2 + |P_-^{nf}|^2$ and $|D_-|^2 = |D_-^f|^2 + |D_-^{nf}|^2$ for the reactions $\pi^- p \to K^- K^+ n$ and $\pi^+ n \to K^- K^+ p$.

for $M > 1200$ MeV. Below 1200 MeV, where D_0 is insignificant, there is only one solution for the S and P waves and this solution shows a large S^* effect in the S_0 amplitude together with a much smaller, but significant P_0 amplitude. Above 1200 MeV the first set of solutions exhibits an enhancement in the S wave near 1300 MeV along with a smooth continuation of the small P wave from the lower-mass region. The second solution shows a sharp rise in P_0 above 1200 MeV and a corresponding falloff of the S_0 amplitude. There is only one D_0 solution (essentially fixed by the $\langle Y_4^0 \rangle$ moment) and it shows the expected enhancement in the region of the f meson near 1300 MeV; we have discussed this D-wave amplitude in detail previously.[1,18]

We show in Figs. 5(b) and 5(d) $|P_-|^2 = |P_-^f|^2 + |P^{nf}|^2$ and $|D_-|^2 = |D_-^f|^2 + |D_-^{nf}|^2$, respectively, for reaction (2); the two ambiguous solutions give similar results for these intensities, to within errors. These $m = 1$ values are small, being typically a few μb/GeV^3, compared to the large $m = 0$ intensities which are ~200 μb/GeV^3.

In order to determine which of the two sets of solutions for reaction (2) is correct, we compare with data on reaction (3), $\pi^- p \to K_S K_S n$. Since these two reactions differ in that $K_S K_S$ contains no L = odd waves, solution 2 with its large P wave would predict a substantial difference between the two reactions, while for solution 1 the difference should be small. In particular,

$$2\langle \sigma Y_2^0 \rangle_{\pi^- p \to K_S K_S n} = (\langle \sigma Y_2^0 \rangle - 0.894\,|P_0|^2)_{\pi^+ n \to K^- K^+ p}\,, \tag{8}$$

where we have neglected the small $|P_\pm|^2$ terms, and the factor of 2 accounts for the unobserved $K_L K_L$ events. In Fig. 6 we show the curves calculated for the right-hand side of Eq. (8), using our two ambiguous solutions, compared to the result of Cason *et al.*[19] While the $K_S K_S$ data are consistent with the small P wave of solution 1,

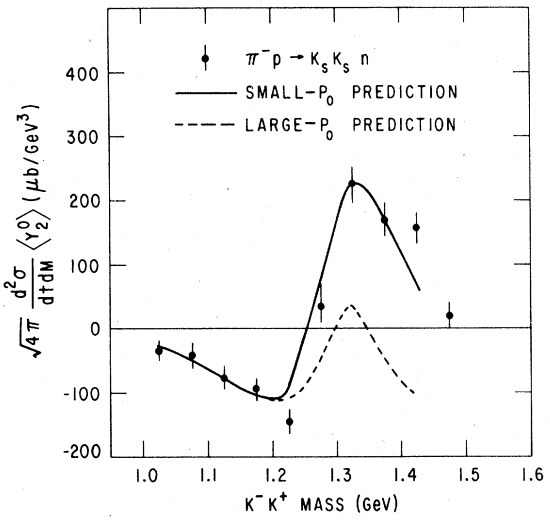

FIG. 6. The $\langle Y_2^0\rangle$ moment for $\pi^- p \to K_S K_S n$ for $|t| < 0.20$ GeV^2 (Ref. 3); the $K_S K_S$ data have been normalized to the $\pi^+ n \to K^- K^+ p$ data using the $\langle Y_4^0\rangle$ moment. The solid curve is the prediction for the $K_S K_S$ $\langle Y_2^0\rangle$ moment based on the $\langle Y_2^0\rangle$ moment from $\pi^+ n \to K^- K^+ p$ using the small P-wave contribution from solution 1, while the dashed curve shows the prediction based on the large P_0 amplitude of solution 2.

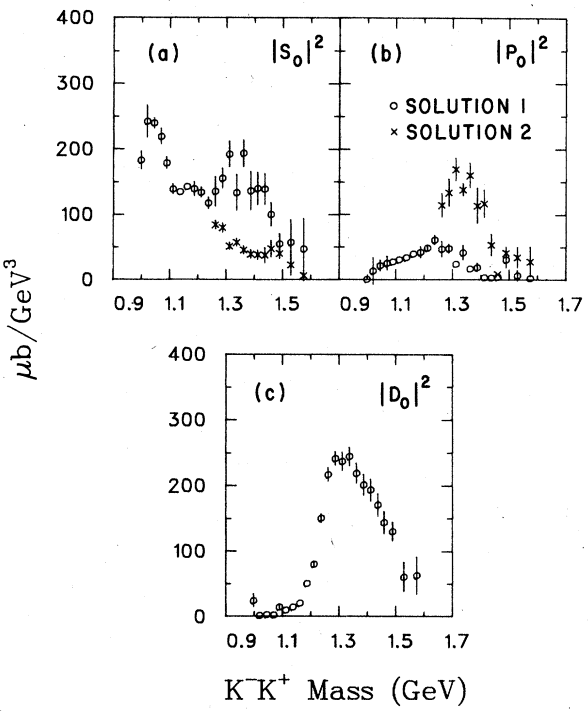

FIG. 7. S_0, P_0, and D_0 intensities for $\pi^- p \to K^- K^+ n$ for $|t| < 0.08$ GeV^2.

the large P wave of solution 2 leads to a gross underestimate of $\langle \sigma Y_2^0\rangle$. We can thus rule out this solution, leaving the solution with the S-wave enhancement at 1300 MeV and the small P-wave amplitude as the correct solution for reaction (2).

We show in Fig. 7 the intensities of S_0, P_0, and D_0 for reaction (1) for $|t| < 0.08$ GeV^2 found by our amplitude analysis. Again there are two sets of solutions and these are qualitatively similar to the solutions for reaction (2), although the substantial quantitative differences do show the presence of interfering $I=0$ and $I=1$ amplitudes. Data on the reaction $\pi^+ n \to K_S K_S p$ could determine the correct solution set for this reaction, in the same way that data on the reaction $\pi^- p \to K_S K_S n$ determined the correct solution for reaction (2), but presently available data are not sufficiently precise to discriminate between our two solutions.[20] Given the similarity of the moments for reactions (1) and (2), one might expect the solution with the large S-wave amplitude also to be the correct one here. The $m=1$ intensities for the two solutions of reaction (1) are again similar to one another within errors and are shown in Figs. 5(a) and 5(c); these intensities are small, with $|D_-|^2$ showing a small enhancement of ~15 μb/GeV^3 in the f-A_2 mass region.

Since the amplitude analysis gives only relative phases, $\phi_S - \phi_D$ and $\phi_P - \phi_D$, we have assumed a Breit-Wigner behavior for the D wave in order to obtain an absolute reference phase. By fitting the $\langle Y_4^0\rangle$ moment with interfering f and f' resonances,[1,18] and assuming an OPEA production phase of 0° for the f, we have extracted the phase ϕ_D shown in Fig. 8. Note that we have found A_2^0 production to be quite small for $|t| < 0.08$ GeV^2, and have ignored possible differences in the D-wave phase between reactions (1) and (2). Since the data only measure terms such as cos (ϕ_S

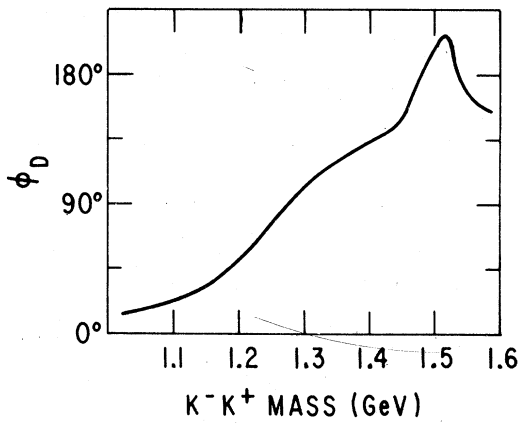

FIG. 8. D-wave phase as determined by fits to the $\langle Y_4^0\rangle$ moment performed in Ref. 1.

$-\phi_D$), each set of solutions for the magnitudes of the amplitudes has two sets of solutions for ϕ_S and ϕ_P. The two sets of phase solutions for reaction (2) are shown in Fig. 9. The two solutions for the S-wave phase determined by Cason *et al.*[3] are consistent with these solutions. One solution exhibits a rapid rise for ϕ_S near 1300 MeV suggestive of a Breit-Wigner-type phase variation; this solution also has a rapid phase variation for ϕ_P. The other solution has both a slowly varying S-wave phase and a slowly varying P-wave phase. For reaction (1) there are four mathematically possible sets of phase solutions, and these are shown in Fig. 10. Solutions 1A and 1B of Fig. 10 arise from solution 1 of Fig. 7, while solutions 2A and 2B arise from solution 2. Solutions 1A and 2A have rapid, Breit-Wigner-type phase variations near 1300 MeV for both ϕ_S and ϕ_P, while the other two solutions have slowly varying phases in this mass region.

Having determined the magnitudes and absolute phases of the amplitudes for each of these solutions, we can now extract the corresponding $I=0$ and $I=1$ S-wave and P-wave helicity-zero $\bar{K}K$ production amplitudes:

$$S_{I=0}=\tfrac{1}{2}(S_{\pi^-p}+S_{\pi^+n}),\quad S_{I=1}=\tfrac{1}{2}(S_{\pi^-p}-S_{\pi^+n}),$$
$$P_{I=0}=\tfrac{1}{2}(P_{\pi^-p}+P_{\pi^+n}),\quad P_{I=1}=\tfrac{1}{2}(P_{\pi^-p}-P_{\pi^+n}), \tag{9}$$

where S_{π^-p} refers to S_0 for reaction (1), etc. Each solution set for S_0, P_0, ϕ_S, and ϕ_P from reaction (1) combined with each solution set from reaction (2) gives one solution for the magnitudes and phases of the $I=0$ and $I=1$ S-wave and P-wave amplitudes. Since we have four mathematically allowed solutions for reaction (1) and two solutions for reaction (2) we obtain eight possible solutions for the isospin amplitudes. There are, in fact, four solutions for the magnitudes of the amplitudes, each of which has two phase solutions, as shown in Figs. 11–14. We have labeled the four solutions for the magnitudes with Roman numerals I–IV, with the corresponding phase solutions denoted by (a) and (b). Table IV gives the

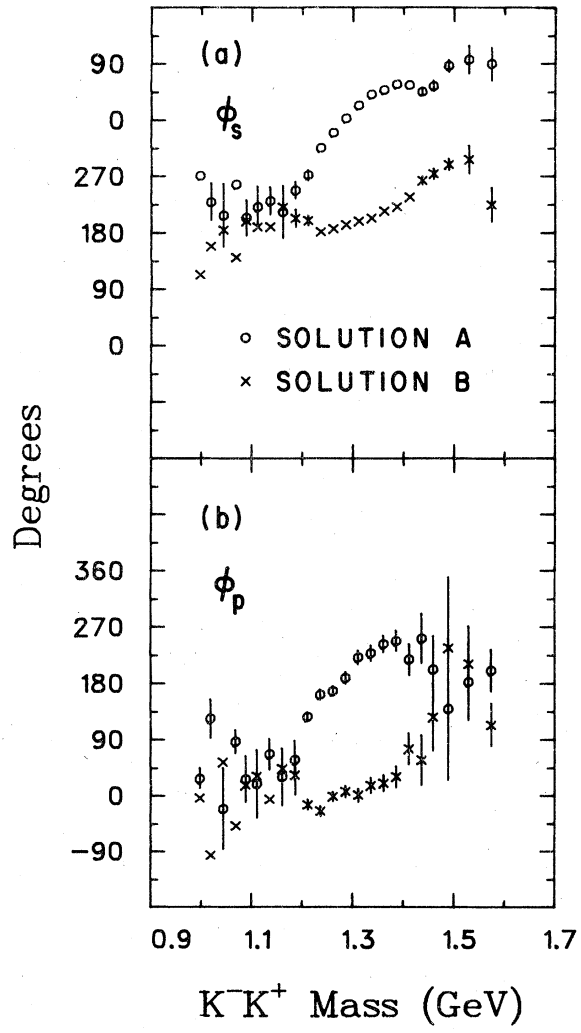

FIG. 9. S-wave and P-wave phases for $\pi^+n\to K^-K^+p$ for $|t|<0.08$ GeV^2. The error bars for both solutions are the same.

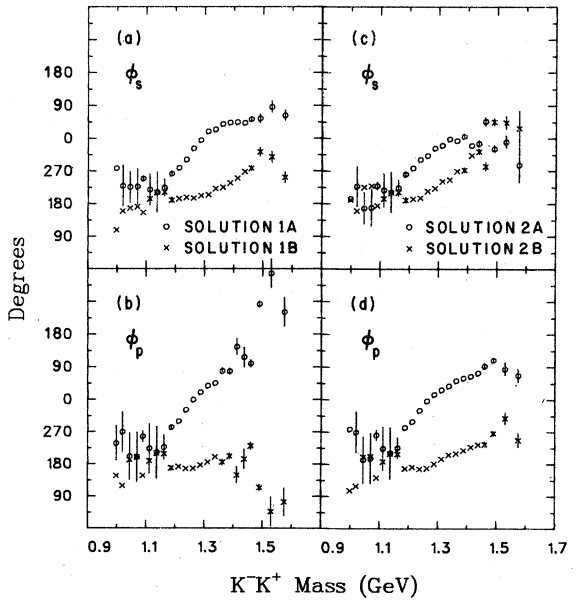

FIG. 10. S-wave and P-wave phases for $\pi^-p\to K^-K^+n$ for $|t|<0.08$ GeV^2. Solutions 1A and 1B for ϕ_S and ϕ_P arise from solution 1 of Fig. 7, while solutions 2A and 2B arise from solution 2 of Fig. 7. The error bars for solutions 1A and 1B, and for 2A and 2B are the same.

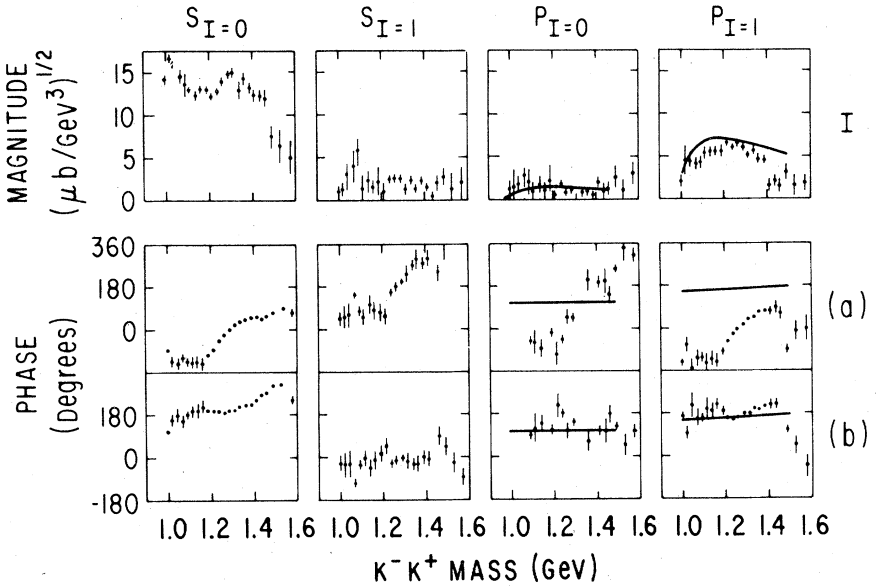

FIG. 11. Solution I results for the $I=0$ and $I=1$ S-wave and P-wave amplitudes for $|t| < 0.08$ GeV^2. The curves superimposed on $P_{I=1}$ represent the behavior for the $I=1$ P-wave amplitude if it were dominated by the high-mass tail of the ρ meson decaying into K^-K^+. The curves on $P_{I=0}$ are an extrapolation of the ω tail. Solution I(b) is the most plausible of the eight solutions (see text).

correspondence between these solutions, which refer to pure isospin states, and solutions described above for the separate reaction amplitudes. Solutions I and II arise from solution 1 of reaction (1) (large S wave near 1300 MeV), while solutions III and IV come from solution 2 (large P wave).

The solutions shown in Figs. 11–14 differ most markedly in the mass region above 1200 MeV. The characteristics of each solution in the region $1200 < M_{\bar{K}K} < 1400$ MeV are summarized in Table V. While the only high-mass structure in solution I is the broad enhancement near 1300 MeV in $S_{I=0}$, solutions II, III, and IV exhibit additional structures in two or more of the waves. All of the solutions except for I(b) indicate rapid phase variations in one or more of the amplitudes.

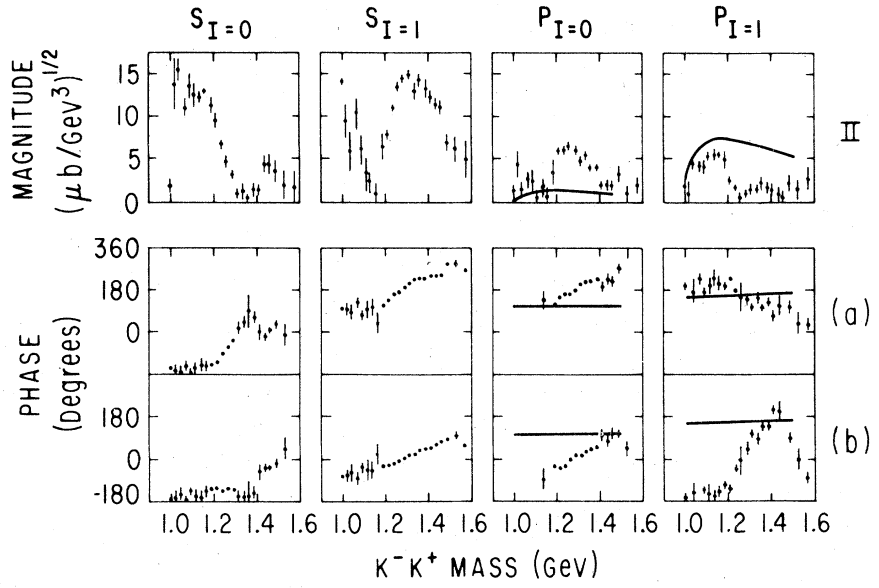

FIG. 12. Solution II results for the $I=0$ and $I=1$ S-wave and P-wave amplitudes for $|t| < 0.08$ GeV^2. See Fig. 11 and text for a discussion of the curves.

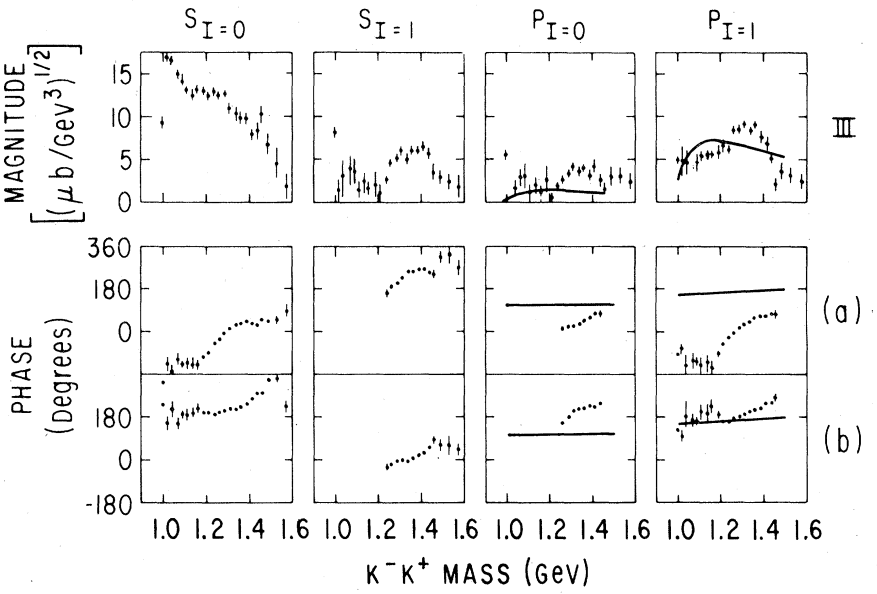

FIG. 13. Solution III results for the $I=0$ and $I=1$ S-wave and P-wave amplitudes for $|t|<0.08$ GeV^2. See Fig. 11 and text for a discussion of the curves.

IV. RESOLUTION OF AMBIGUITIES

Given the eight mathematically possible solutions, and lacking additional data from other reactions such as $\pi^+ n \to K_S K_S p$, physics arguments are required to distinguish the correct solution. Taken together the physics arguments point very strongly toward solution I(b) (derived from solutions 1B of each of the reactions separately).

To summarize these arguments, we note first that solutions I(a) and I(b) are the only ones derived from analogous solutions to the separate reactions (cf. Table IV). It would indeed be unexpected if the amplitudes for the two reactions were radically different, but fortuitously happened to give qualitatively similar observables. Solutions I(a) and I(b) also have the desirable feature that the even-G-parity amplitudes are much larger than the odd ones, as expected from OPEA

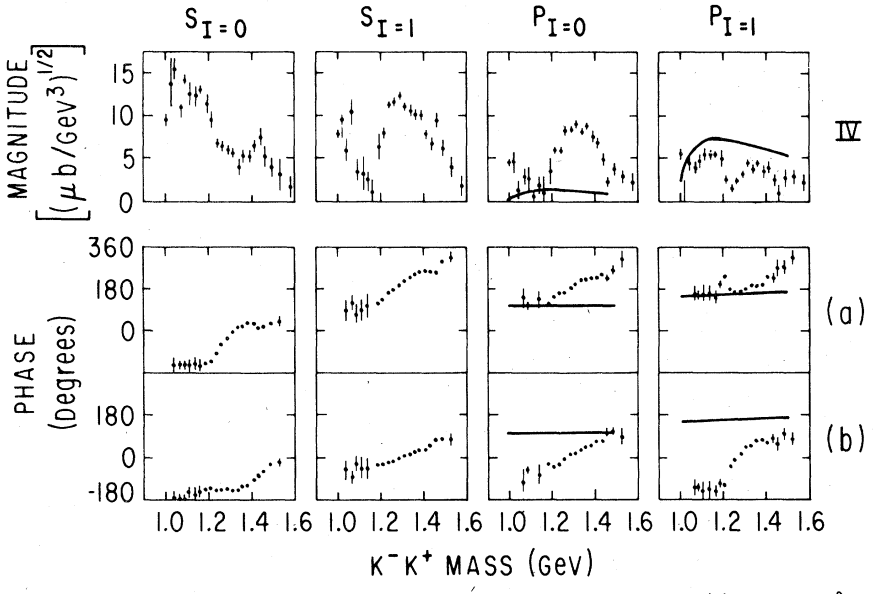

FIG. 14. Solution IV results for the $I=0$ and $I=1$ S-wave and P-wave amplitudes for $|t|<0.08$ GeV^2. See Fig. 11 and text for a discussion of the curves.

TABLE IV. Map showing how the eight solutions for the $I=0$ and $I=1$ S and P waves arise from the various $\pi^-p \to K^-K^+n$ and $\pi^+n \to K^-K^+p$ solutions.

	I		II		III		IV	
	(a)	(b)	(a)	(b)	(a)	(b)	(a)	(b)
π^-p solution	1A	1B	1B	1A	2A	2B	2B	2A
π^+n solution	1A	1B	1A	1B	1A	1B	1A	1B

dominance at small t. As discussed below, they are the only solutions that exhibit reasonable t dependence for the S and P waves, consistent with the phenomenology of π and B exchange processes. Solutions II(a) and II(b) are mathematical inversions of solution I, in which the amplitudes with B-exchange quantum numbers behave like π exchange, while the amplitudes with π-exchange quantum numbers have the characteristics of B exchange. Solutions III and IV exhibit highly anomalous t dependences in some of the amplitudes. Moreover, as shown below, the S waves for solutions III and IV extrapolate to completely different values at the pion pole for reactions (1) and (2), a behavior which is not allowed if OPEA provides any significant contribution to the production mechanism. Finally, taking solutions I(a) and I(b) to be the only reasonable choices, we argue that only solution I(b) has acceptable phase behavior; the P-wave phases in this solution are consistent with the ρ and ω Breit-Wigner tails, whereas in solution I(a) all of the S- and P-wave amplitudes exhibit rapid phase variations for which no physical explanation is apparent.

We now discuss some of these arguments in more detail, namely, the t dependence of the larger amplitudes, the OPEA S-wave extrapolation, and the parametrization of the smaller amplitudes as Breit-Wigner tails.

TABLE V. Approximate magnitude A of the amplitudes averaged over $|t|<0.08$ GeV^2 at 1300 MeV, and approximate phase changes $\Delta\phi$ of the large amplitudes from 1200 to 1400 MeV. The units are $(\mu b/GeV^3)^{1/2}$ and degrees, respectively. For comparison, the magnitude of D_0 is ~15 $(\mu b/GeV^3)^{1/2}$ and the phase advance ~80°.

Solution		$S_{I=0}$ A	$S_{I=0}$ $\Delta\phi$	$S_{I=1}$ A	$S_{I=1}$ $\Delta\phi$	$P_{I=0}$ A	$P_{I=0}$ $\Delta\phi$	$P_{I=1}$ A	$P_{I=1}$ $\Delta\phi$
I	(a)	15	135	2	230	1	200	6	125
	(b)		30		−10		0		40
II	(a)	2	180	15	100	6	75	1	−90
	(b)		15		70		90		270
III	(a)	11	130	6	100	4	45	9	120
	(b)		40		45		70		50
IV	(a)	6	160	11	110	9	80	4	20
	(b)		10		60		90		180

A. t dependence

Since the waves $S_{I=0}$ and $P_{I=1}$ can couple to π exchange, we would expect these amplitudes to exhibit the steep t dependence for small t characteristic of OPEA, roughly $d\sigma/dt \propto e^{12t}$. On the other hand, the waves $S_{I=1}$ and $P_{I=0}$ can be produced only by $G=+1$ unnatural-parity exchanges such as the B trajectory. Processes which involve B exchange, such as $\pi^-p \to \omega n$ and $\pi^-p \to A_2^0 n$, are known to have a substantially flatter t dependence,[21-24] roughly $e^{3.5t}$, and we would expect $S_{I=1}$ and $P_{I=0}$ to have a similar t dependence.

To determine the t dependence of the S and P waves in our solutions, we have repeated the amplitude analysis as a function of t in the mass region 1250 to 1450 MeV, where the solutions are ambiguous. The D wave, which is known to be dominated by π exchange in the reaction $\pi^-p \to \pi^-\pi^+n$,[12,15] serves as a calibration for the OPEA t dependence. The slope parameters for $\pi^-p \to \rho^0 n$ and $\pi^-p \to fn$ in the t-channel helicity-0 states are found to be very nearly equal at 17 GeV/c. Extrapolating to our energy,[12] we would expect the D-wave production slope to be ~12 GeV^{-2} over the range $0.04<|t|<0.20$ GeV^2. The K^-K^+ D-wave intensities are displayed in Fig. 15; exponential slopes of 10.5 ± 0.5 and 9.5 ± 1.3 GeV^{-2} are observed for reactions (1) and (2), respectively. These values are somewhat low, but are reasonably consistent with the OPEA

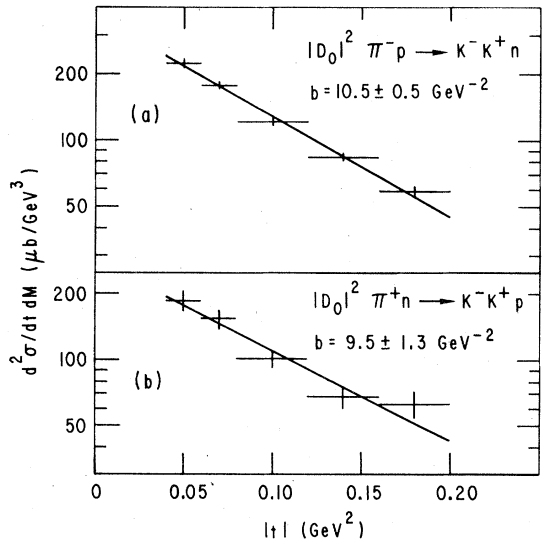

FIG. 15. $|D_0|^2$ for the K^-K^+ mass region $1250<M<1450$ MeV as a function of t for reactions (1) and (2). The lines shown are fits to Ae^{bt}, with the parameters b shown in the figure.

expectation.

The $|S_0|^2$ t distributions of reactions (1) and (2) in this mass region are shown in Fig. 16. We obtain slopes of 16.5 ± 1.6 and 4.6 ± 1.2 GeV^{-2}, respectively, for solutions 1 and 2 of reaction (1), and 7.4 ± 1.0 GeV^{-2} for solution 1 of reaction (2), fitted over the range $0.04 < |t| < 0.20$ GeV^2. Note that the t distribution for reaction (2) is much flatter than expected for OPEA, while for solution 1 of reaction (1) it is much steeper. The large difference in slopes between the two reactions is due to interference between the OPEA amplitude $S_{I=0}$ and the flatter B-exchange $S_{I=1}$ amplitude. A simple average of the slopes, which projects out the behavior of the dominant $|S_{I=0}|^2$ contribution, is consistent with OPEA (~11 GeV^{-2}).

We have constructed the pure isopin amplitudes corresponding to solutions I–IV as functions of t in the high-mass region, and the resulting slopes are summarized in Table VI. The $I=0$ S-wave intensity from solution I is shown in Fig. 17(a); the slope of this t distribution, fitted over the range $0.04 < |t| < 0.20$ GeV^2, is 11.0 ± 0.8 GeV^{-2},

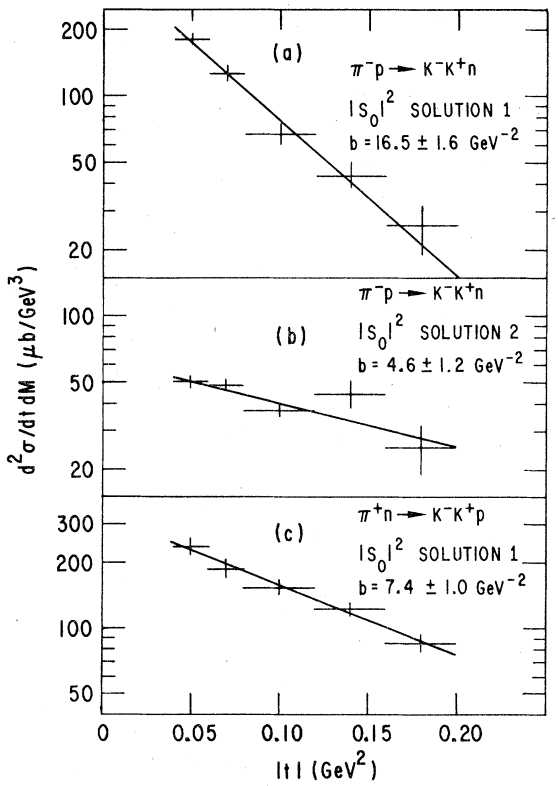

FIG. 16. $|S_0|^2$ for the K^-K^+ mass region $1250 < M < 1450$ MeV as a function of t. (a) and (b) are the two solutions for reaction (1) while (c) is the only correct solution for reaction (2). The lines shown are fits to Ae^{bt}, with the parameters b shown in the figure.

TABLE VI. Slopes of the t distributions for the large amplitudes averaged over the K^-K^+ mass region $1250 < M < 1450$ MeV. The intensities were fitted over the range $0.04 < |t| < 0.20$ GeV^2 to the form Ae^{bt}. Also shown are the values expected on the basis of similar reactions, such as f production for the OPEA amplitudes and ω and A_2 production for non-OPEA amplitudes. Units are GeV^{-2}.

Solution	$S_{I=0}$	$S_{I=1}$	$P_{I=0}$	$P_{I=1}$
I	11.0 ± 0.8	flat	flat	7.6 ± 1.6
II	flat	11.0 ± 0.8	7.6 ± 1.6	flat
III	5.1 ± 0.7	16.8 ± 1.6	30.7 ± 5.5	19.0 ± 1.4
IV	16.8 ± 1.6	5.1 ± 0.7	19.0 ± 1.4	30.7 ± 5.5
Expected	~10	~flat	~flat	~10

in good agreement with the expected OPEA behavior. In contrast, the $I=1$ S wave from solution I, shown in Fig. 17(c), has a rather flat t dependence with a turnover in the forward direction. The dashed curves in Fig. 17(c) indicate the t dependence expected for B exchange, specifically $\rho_{00}(d\sigma/dt)$ for the reaction $\pi^-p \to \omega n$ (Refs. 11 and 23) (we have plotted both s- and t-channel ω-production cross sections, since it is not clear which one is appropriate for predicting the behavior of S-wave production). Although the ω-production cross section does not exhibit a forward turnover, the B-exchange component of ω production (as opposed to the Z-exchange part) is expected to vanish near $t=0$. We are mainly sensitive to the S- and P-wave amplitudes which are spin coherent with the D wave, namely the π and B exchanges, and this presumably accounts for the turnover in our $I=1$ S-wave amplitude. The t distributions for solution II may be obtained by interchanging the $I=0$ and $I=1$ waves of solution I. Thus, solution II is a mathematical inversion of solution I, with $S_{I=1}$ having an OPEA-like t distribution and $S_{I=0}$ behaving like a B-exchange amplitude, just the opposite of the expectation.

The t dependence of $|P_{I=1}|^2$ for solution I is shown in Fig. 17(b); the slope of 7.6 ± 1.6 GeV^{-2} is flatter than expected for OPEA (since the P wave has a relatively small amplitude compared to the S wave just discussed, it may well have non-negligible contributions from other processes). The $I=0$ P wave for solution I is quite small and is consistent within errors with the slowly varying shape of the helicity-0 ω-production cross section indicated by the dashed curve in Fig. 17(d). Again, solution II represents a simple interchange of $I=0$ and 1 amplitudes, a mathematical possibility which results in unreasonable t dependences.

The t dependences of the $I=0$ and 1 S- and P-wave intensities in solutions III and IV are shown in Fig. 18 and are summarized in Table VI. These

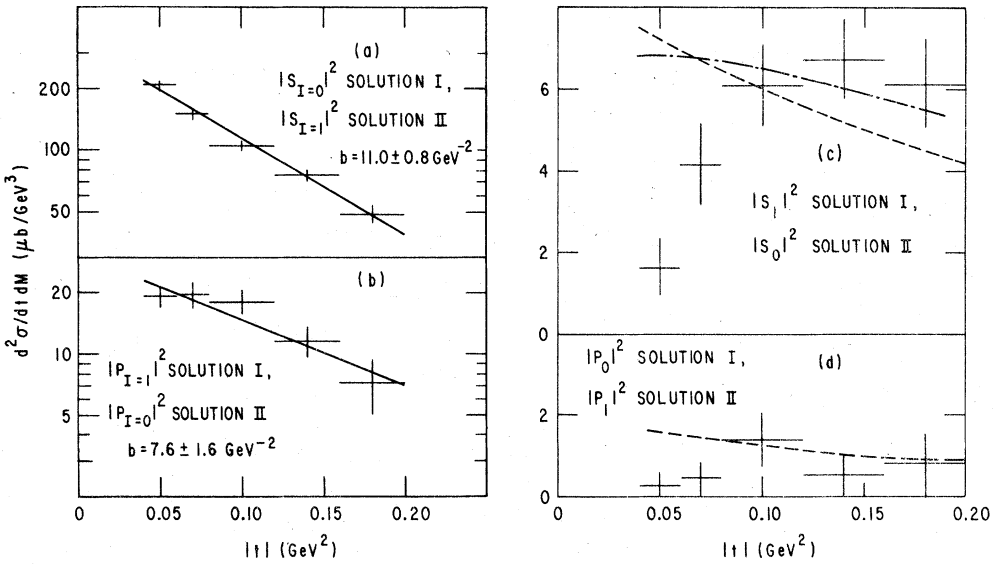

FIG. 17. The t dependence of the S- and P-wave intensities averaged over $1250 < M < 1450$ MeV for solutions I and II. The dashed (dot-dashed) curves give the t- (s-) channel shape of the cross section $\rho_{00}d\sigma/dt(\pi^-p \to \omega n)$. The dashed curve in (d) is normalized to the $\omega \to \bar{K}K$ contribution to $|P_{I=0}|^2$. The solid lines shown in (a) and (b) are fits to Ae^{bt}, with the parameters b shown in the figure.

solutions exhibit quite anomalous behavior. In particular, note the slopes of 19.0 ± 1.4 and 31 ± 6 GeV^{-2} for the P waves in these solutions. These slopes are much larger than observed for any normal peripheral processes, even OPEA, diffraction, etc.

A summary of fitted and expected slopes is shown in Table VI; only solution I, the solution with the large $I=0$ S-wave enhancement at 1300 MeV, exhibits t dependences consistent with the expected production mechanisms.

B. OPEA extrapolation

As a consistency check we have done an extrapolation to the pion pole of $|S_0|^2$ from the individual reactions (1) and (2) for the mass region $1250 < M < 1450$ MeV. If production is dominated by OPEA, the correct solutions should extrapolate to the same value at the pole, namely

$$F(m_\pi^2) = \lim_{|t| \to -m_\pi^2} \frac{(|t| + m_\pi^2)^2}{|t|} \frac{d^2\sigma}{dt\,dM}. \qquad (10)$$

Figure 19(a) shows a linear extrapolation for the only possible $|S_0|^2$ solution for reaction (2). The value extrapolated to the pion pole is 24.4 ± 2.4 μb/GeV. Figures 19(b) and (c) show the extrapolation for the two possible solutions for reaction (1). Solution 1 extrapolates to 22.2 ± 1.5 μb/GeV, while solution 2 extrapolates to 4.0 ± 0.7 μb/GeV. Evidently reactions (1) and (2) agree at the pion pole only for solution 1. Thus, if OPEA is assumed to be a significant part of the production mechanism, then only solutions I and II, which are based on solution 1, are viable, and solutions III and IV can be rejected. Conversely, the agreement of reactions (1) and (2) at the pion pole strongly supports the hypothesis that the $I=0$ S wave is dominant and is produced mainly by OPEA.

C. Extrapolation of the known resonance tails

As a further check on the validity of solution I, we have calculated the behavior expected for the $I=1$ P-wave amplitude if it were dominated by the high-mass tail of the ρ meson decaying into K^-K^+, with $\rho\bar{K}K$ coupling given by SU(3).[25] Both the magnitude and phase expected for the $I=1$ P-wave amplitude have been calculated, and these are shown as the solid curves in Figs. 11–14. Only our favored solution, solution I, is in reasonable agreement with the predicted magnitude up to 1400 MeV. The existence of a solution in agreement with the ρ tail has been previously noted by Morgan.[8] Requiring agreement of the $I=1$ P-wave phase with the phase expected from the ρ tail chooses solution I(b), the solution with slowly varying S- and P-wave phases in the 1300-MeV mass region.

The $I=0$ P wave has the quantum numbers of the ω. If the K^-K^+ waves were given entirely by the tails of the ρ and ω, we would expect the ratio of the amplitudes in the $\bar{K}K$ channel to be

$$\frac{P_{I=0}}{P_{I=1}} = \frac{A_\omega}{A_\rho}\left(\frac{M_\rho^2 - M^2 - iM_\rho\Gamma_\rho}{M_\omega^2 - M^2 - iM_\omega\Gamma_\omega}\right)\frac{g_{\omega K^-K^+}}{g_{\rho K^-K^+}}, \qquad (11)$$

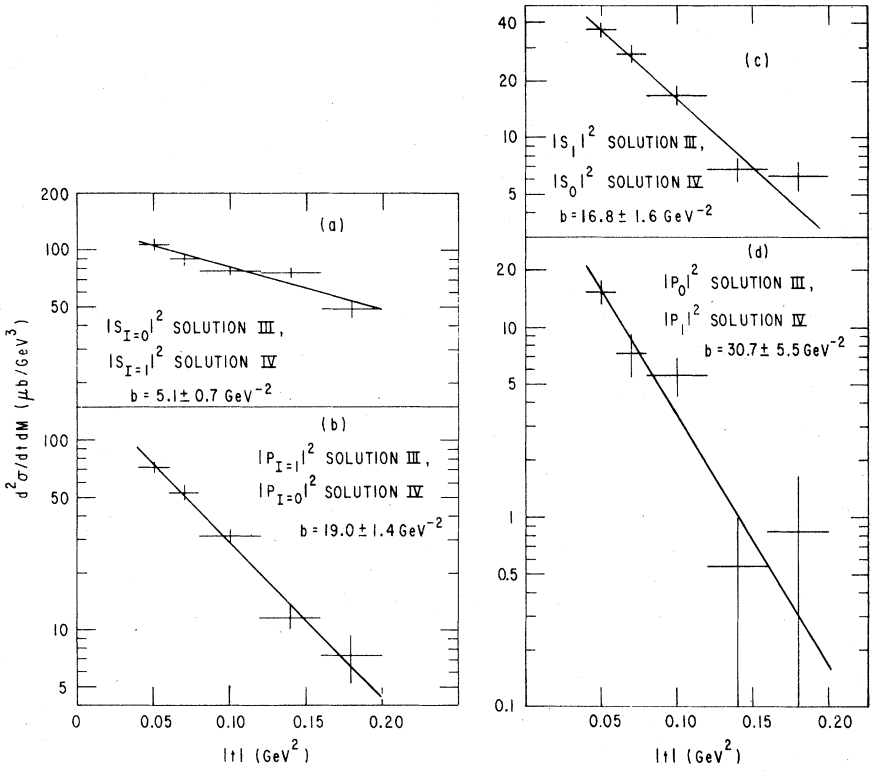

FIG. 18. The t dependence of the S- and P-wave intensities averaged over $1250 < M < 1450$ MeV for solutions III and IV. The lines shown are fits to Ae^{bt}, with the parameters b shown in the figure.

where $A_\omega(A_\rho)$ are the $\omega(\rho)$ production amplitudes measured in the 3π (2π) final states; $g_{\omega K^- K^+}$ and $g_{\rho K^- K^+}$ are the decay couplings, which are predicted by SU(3) to be equal, assuming ideal mixing for the vector nonet. The ratio of propagators becomes equal at high masses, away from resonance, and an adequate approximation above $\bar{K}K$ threshold is $P_{I=0}/P_{I=1} = A_\omega/A_\rho$.

From analysis of ρ-ω interference in $\pi^-\pi^+$ production,[12] both the magnitude and phase of the ratio A_ω/A_ρ are known as functions of t. In particular, the phase of A_ω relative to A_ρ is around $-60°$ for the t-channel $m = 0$ amplitude for $|t| < 0.4$ GeV^2. The resulting predictions for the magnitude and phase of $P_{I=0}$ are indicated in Figs. 11–14 and Fig. 17(d). As with the ρ tail, it is clear that the ω tail is consistent with $P_{I=0}$, but only for solution I(b).

An estimate of the $I = 1$ S-wave cross section was made by Irving,[26] assuming that it arises from the production and decay of the $\delta(980)$ meson. For the region $M < 1200$ MeV and $|t| \leq 0.08$ GeV^2 he predicts 0.08 μb, in good agreement with the 0.11 ± 0.05 μb given by solution I.

Thus, we conclude that solutions I(a) and I(b) are the only solutions with phenomenologically sensible behavior for the π- and B-exchange waves, and solution I(b) is unique in giving P waves consistent with expected tails of the known vector mesons.

V. COMPARISON WITH OTHER $\bar{K}K$ ANALYSES

The most intriguing feature of our favored solution I(b) is the broad enhancement in the $I = 0$ S wave around 1300 MeV (see Fig. 11). While it is tempting to characterize this enhancement as a resonance, the absence of phase variation in $S_{I=0}$ at 1300 MeV argues against a simple resonance interpretation. The nature of this enhancement is further clouded by observations from other experiments. For example, Cason *et al.*[3] have argued that the S-wave t distribution in the reaction $\pi^- p \to K_S K_S n$ is anomalously flat and that the overall phase of the S wave would be $\approx 90°$ in the 1300-MeV region for a π-exchange production mechanism, not $\approx 180°$ as observed. They have concluded that the S-wave enhancement does not couple to $\pi\pi$, and have suggested that the effect may be confined to the $I = 1$ state. In an analysis which appears to support the arguments of Cason *et al.*,[3] Martin *et al.*[5] have presented evidence for an $I = 1$ S-wave enhancement around 1300 MeV in the $K^- K^0$ system produced in the reaction $\pi^- p \to K^- K_S^0 p$.

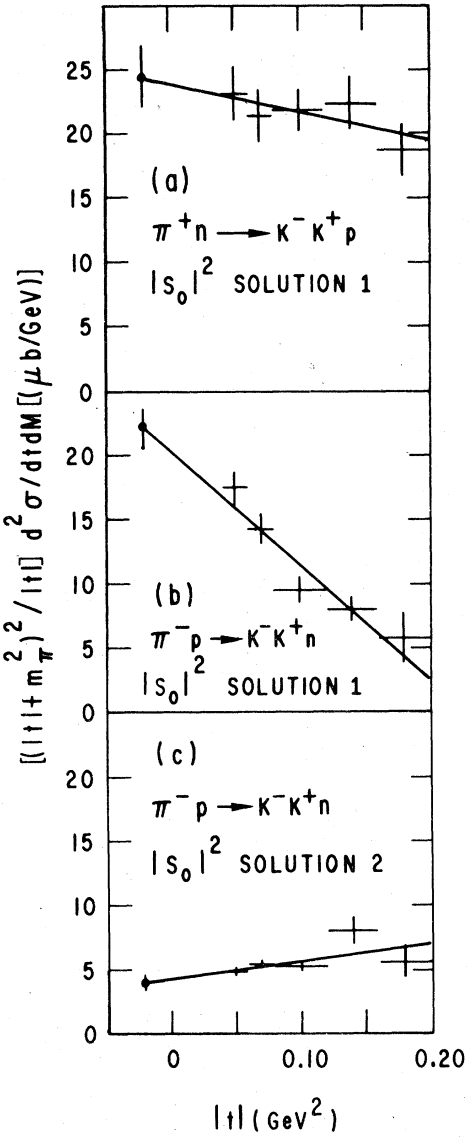

FIG. 19. Extrapolation to the pion pole of $|S_0|^2$ averaged over $1250 < M < 1450$ MeV.

In this section, we examine the t distributions in K^-K^+ and K_SK_S final states, demonstrating that there are no unusual features that would undermine the overall picture which we have established in Sec. IV. We also compare our interpretation of the S-wave enhancement with the K^-K^0 amplitudes found by Martin *et al.*[5] The explanation of the $I=0$ S-wave phase in the 1300-MeV region is taken up in Sec. VI.

A. Momentum-transfer dependence in $(\bar{K}K)^0$ production

Cason *et al.*[3] argued that the 1300-MeV enhancement is produced with a flatter t dependence than the $(\bar{K}K)^0$ S wave near threshold, indicating a difference in production mechanism between the two regions. To compare these mass regions, we have performed a simplified analysis of the S wave near threshold ($1030 < M < 1100$ MeV) using our data from reactions (1) and (2). The differential cross sections, which are well determined out to $|t| \approx 0.4$ GeV^2 (Ref.1), can be parametrized adequately with S- and P-wave contributions. We constrained the P waves to satisfy our parametrization for the ρ and ω tails, and we fixed the relative phases of $S_{I=0}$ and $S_{I=1}$ from the small-t amplitude analysis. The resulting S-wave intensities are shown in Fig. 20. For comparison we also plot the S-wave cross sections from solution I(b) for the 1300-MeV region, together with the distributions expected for π and B exchanges. As in Fig. 17(c), the B-exchange shape is taken from $\rho_{00}\, d\sigma/dt$ for the reaction $\pi^- p \rightarrow \omega n$.

From Fig. 20 we conclude that $|S_{I=0}|^2$ may be

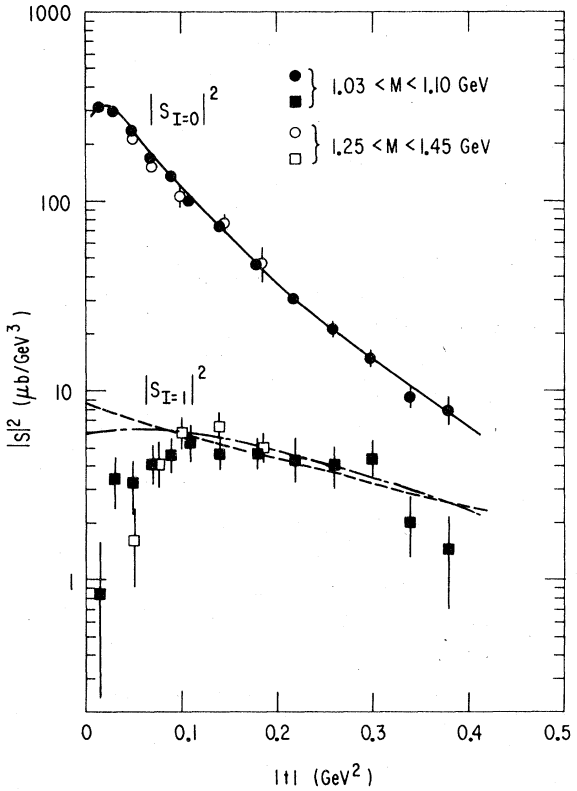

FIG. 20. The $I=0$ and $I=1$ S-wave cross sections in the threshold region $1030 < M < 1100$ MeV (solid points) and in the region $1250 < M < 1450$ MeV (open points). The solid curve is an OPEA fit to the $I=0$ S wave using Eq. (7a) in the threshold region ($B_S = 2.9$ GeV^{-2}); the dashed (dot-dashed) curve is the shape of the t- (s-) channel cross section for $\rho_{00} d\sigma/dt(\pi^- p \rightarrow \omega n)$ from Ref. 23.

slightly flatter in the high-mass region. However, in terms of an exponential fit of the form $d\sigma/dt \sim Ae^{bt}$, the slope b changes from 12.1 ± 0.3 GeV^{-2} near threshold to $b = 11.0 \pm 0.8$ GeV^{-2} in the high-mass region, fitted over the range $0.04 < |t| < 0.20$ GeV^2. While a relative change in slope of $\approx 10\%$ can certainly alter the mass spectrum significantly at large t, it does not imply that the production mechanisms are different in the two mass regions. To parametrize the cross sections more precisely over a wider t range, as shown in Fig.20, we have fitted $|S_{I=0}|^2$ to the OPEA form of Eq. (7a). In Fig. 21(a) we plot the resulting OPEA slopes as

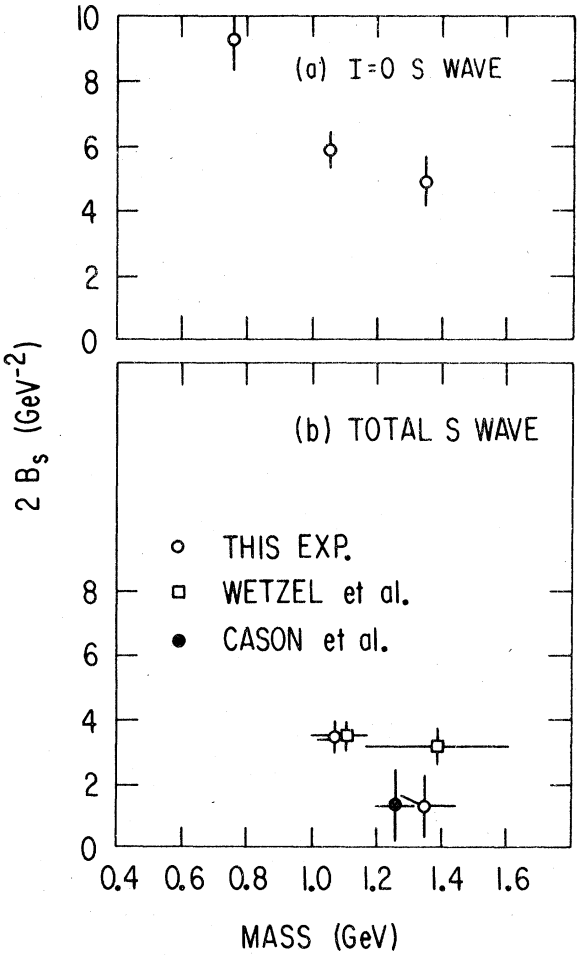

FIG. 21. (a) OPEA slope parameters for the $I = 0$ S wave obtained from fits of the form given by Eq. (7a). Note that we have plotted $2B_S$, which is directly related to the cross-section slope. The lowest-mass point represents dipion production (see Ref. 12) for $|t| < 0.28$ GeV^2. The two high-mass points are from fits to $|S_{I=0}|^2$ for $|t| < 0.2$ GeV^2. (b) OPEA slopes for reaction (2), $|t| < 0.2$ GeV^2 (this experiment) and reaction (3), $|t| < 0.5$ GeV^2; data are from Wetzel *et al.* (Ref. 4) and Cason *et al.* (Ref. 3).

functions of mass, including the slope for S-wave dipion production in the ρ region from Ref. 12. We see that the change in slope going from the S^* to the 1300-MeV region is less than the overall slope difference between the $\pi\pi$ and $\bar{K}K$ S waves. The reason for the slope-mass correlation is unclear, but the modest variation observed over the $\bar{K}K$ mass spectrum does not suggest any drastic change from OPEA production in the high-mass region.

Figure 20 also shows $|S_{I=1}|^2$ as a function of t, both near threshold and in the high-mass region. These data are consistent in shape with ω production in both mass regions, and do not exhibit important slope-mass correlations. Note that if ω production can be taken as a guide, the $I = 0$ S wave is likely to dominate over $S_{I=1}$ for all momentum transfers ($|t| < 0.5$ GeV^2) accessible to present $(\bar{K}K)^0$ experiments.

Thus, we have shown that the $I = 0$ S wave has an OPEA-like t dependence over the whole $\bar{K}K$ mass spectrum. Regarding the argument of Cason *et al.*[3] that the K_SK_S S wave in reaction (3) has an anomalously flat t dependence around 1300 MeV, we first note that reactions (2) and (3) should exhibit the same S-wave behavior due to charge symmetry. We have already shown that $|S|^2$ in reaction (2) has a t dependence which is flatter than OPEA in the 1300-MeV region (cf. Fig. 16), and that this is due to constructive interference between the $I = 0$ and $I = 1$ S waves. However, given the relative phases between $S_{I=0}$ and $S_{I=1}$ from solution I(b), we expect this flatter t dependence to occur over the entire $(\bar{K}K)^0$ mass spectrum for reactions (2) and (3), not just in the 1300-MeV region.

To search for anomalous t dependence in reactions (2) and (3), we have again compared the t distributions near threshold with those in the high-mass region. Figure 21(b) shows the OPEA slope parameters obtained by Wetzel *et al.*[4] for reaction (3); they indicate little if any slope-mass correlation in K_SK_S production. Also shown are our OPEA fits to the data from reaction (2) and to the K_SK_S S-wave cross section of Cason *et al.*[3] These fits indicate a modest slope-mass correlation for reactions (2) and (3); this effect is probably due mainly to the slope-mass correlation found for the dominant $I = 0$ S wave [Fig. 21(a)]. Finally, Fig. 22 shows the S-wave cross section in the high-mass region obtained by Cason *et al.*, as a function of t, compared with our data from reaction (2) and the OPEA parametrization corresponding to Fig. 21(b). As expected from charge symmetry, reactions (2) and (3) are consistent within errors. Originally, Cason *et al.* reported a rather flat slope for their data from a fit to $|S|^2$

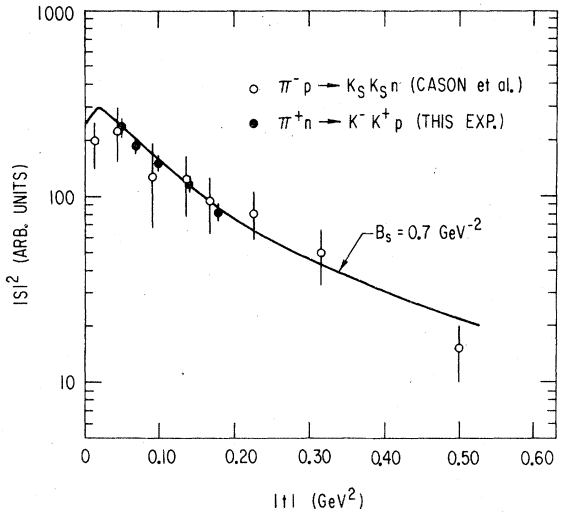

FIG. 22. Differential cross section for the K_SK_S S wave in the mass region $1220 < M < 1320$ MeV from Ref. 3, together with the S-wave intensity obtained from our data on reaction (2) in the region $1250 < M < 1450$ MeV. The OPEA curve is based on Eq. (7a), with $B_S = 0.7$ GeV^{-2}.

$\sim Ae^{bt}$, namely, $b = 3.7 \pm 0.8$ GeV^{-2}; their fit covered only part of the t range ($0.06 < |t| < 0.36$ GeV^2), whereas the OPEA fit in Fig. 22 appears to be adequate over the entire t range.

We conclude that there are no significant anomalies in the S-wave t distributions in any of the $(\bar{K}K)^0$ data. The dominant $I = 0$ S wave shows a modest slope-mass correlation, but this by itself does not argue against OPEA dominance. The smaller $I = 1$ S wave has the nearly flat t dependence expected of a B-exchange process, with no indication of a slope-mass correlation. The $S_{I=0}$-$S_{I=1}$ interference results in a flatter t dependence for both reactions (2) and (3) than would be expected for OPEA alone. The flattening is observed in both reactions, and there is no evidence that it is confined to the 1300-MeV region.

B. Comparison with $(\bar{K}K)^-$ production

In order to isolate the $I = 1$ S wave, Martin *et al.*[5] performed an amplitude analysis of reaction (4), $\pi^- p \to K^- K^0 p$, at 10 GeV/c. Their analysis illustrates some important technical difficulties in dealing with charged $\bar{K}K$ production, which are absent in the neutral mode. Recall that in $(\bar{K}K)^0$ production, the natural-parity-exchange (NPE) cross section is small and easily removed. Furthermore, the S wave accounts for nearly half of the cross section, and OPEA dominates the unnatural-parity-exchange (UPE) observables, allowing some simplifying assumptions. By contrast, reaction (4) is dominated by NPE production of the A_2^-. For example, around 1300 MeV $\bar{K}K$ mass, the UPE cross section including the S wave is only ~15% of the total.[5] Since NPE and UPE amplitudes do not interfere, the large NPE cross section must in effect be subtracted off to expose the UPE components. Within the UPE sector, only $P_{I=1}$ can be produced by π exchange. The $I = 1$ S and D waves require B or Z exchange, along with possible $I = 0$ exchanges (e.g., $\eta, D, E \cdots$). As a result, the nucleon-helicity flip and nonflip amplitudes are likely to be equally important, and no simplifying assumption of spin coherence can be made. Thus, while the magnitudes of the amplitudes can be estimated, the relative phases cannot be determined without a specific model for the nucleon spin dependence.

Martin *et al.*[5] obtained two solutions for the magnitudes of the UPE S_0 and P_0 waves in reaction (4), for the t range $0.07 < |t| < 1$ GeV^2. These solutions differ essentially in the interchange of $|S_0|$ and $|P_0|$. As shown in Fig. 23, the "large" wave, which they prefer to identify with S_0, shows a possible enhancement around 1300 MeV. Note that this enhancement coincides in mass with the A_2^-; such a peak might be expected if there were any feedthrough from the dominant NPE to the

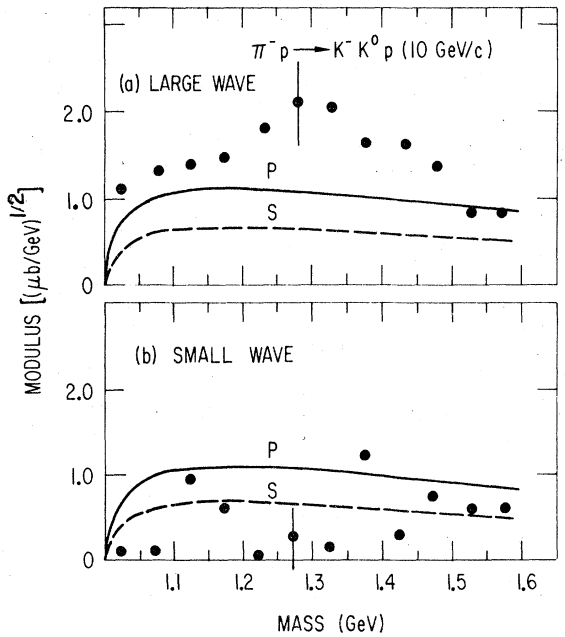

FIG. 23. "Large" and "small" waves from the amplitude analysis of the S and P waves in $\pi^- p \to K^- K^0 p$ of Ref. 5. The curves represent extrapolations of the $I = 1$ S wave in K^-K^+ (dashed) and of the $I = 1$ P wave associated with the ρ^- tail (solid). Representative error bars are shown for a few points.

UPE cross section.

Using measured cross sections for $\rho^{\pm}$ production in the reactions $\pi^{\pm}p \to \pi^{\pm}\pi^0 p$,[27] we have calculated the ρ^--tail contribution to $P_{I=1}$ for reaction (4). This ρ^- tail is depicted by the solid curves in Fig. 23. We have also extrapolated the $I=1$ S wave found in our analysis of $(\overline{K}K)^0$ production to 10 GeV/c, using ω production to constrain the energy and t dependence; this is represented by the dashed curves in Fig. 23. Of course, due to the OPEA dominance, $S_{I=1}$ found in $(\overline{K}K)^0$ represents mainly the B-exchange amplitude, whereas in $(\overline{K}K)^-$ both B and Z exchanges can be important for the S wave. For brevity we will henceforth refer to $S_{I=1}$ from $(\overline{K}K)^0$ as "S_B." Inspection of Fig. 23 reveals two important features. First, the threshold behavior predicted for S and P waves is very similar. Martin *et al.*[5] originally argued that the rapid rise of the "large" wave above threshold provided evidence that it was an S wave and not a P wave. However, the ρ^- tail is expected to show a sharp rise at threshold, and consequently the threshold behavior cannot be used to distinguish the S and P waves. Second, neither wave agrees particularly well with the predicted ρ^- tail. Owing to this discrepancy, Martin and Ozmutlu[16] repeated the amplitude analysis of reaction (4), this time fixing the P wave to agree with the ρ^- tail. They found that the ρ^- tail alone was too small to account for all of the UPE S- and P-wave production, and that the residual S wave is similar to the large wave in Fig. 23, including the enhancement at 1300 MeV.

The t dependence of the large wave,[28] for $1.2 < M_{\overline{K}K} < 1.4$ GeV, is shown in Fig. 24; to obtain this t dependence, Martin *et al.*[28] fixed the "small" wave at zero, but the results are quite similar if the small wave is fixed by the ρ^- tail.[16] Also shown are the expected intensities for the ρ^- tail, S_B, and the A_2^- production amplitudes. We note the following features. (1) The large wave has t dependence similar to the ρ^- tail (solid curve), although the ρ^- tail, even with the expected S_B contribution added (dot-dashed curve), is too small by a factor of 2 in cross section. (2) The large wave has a much steeper t dependence than S_B alone (dashed curve). Thus, if the large wave is indeed an S wave, then it is not produced by B exchange and cannot be identified simply with S_B. (3) The UPE A_2^- production cross section found by Martin *et al.*[28] in the same analysis (dotted curve) has the same t dependence as S_B. Thus, the B-exchange behavior consistently describes a variety of UPE processes, including $\pi^-p \to A_2^-p$, $\pi^+n \to A_2^0p$,[22] $\pi^-p \to \omega n$, and $S_{I=1}$ and $P_{I=0}$ production in reactions (1)–(3). We know of no process, in which B and Z are the allowed exchanges, that exhibits the steep

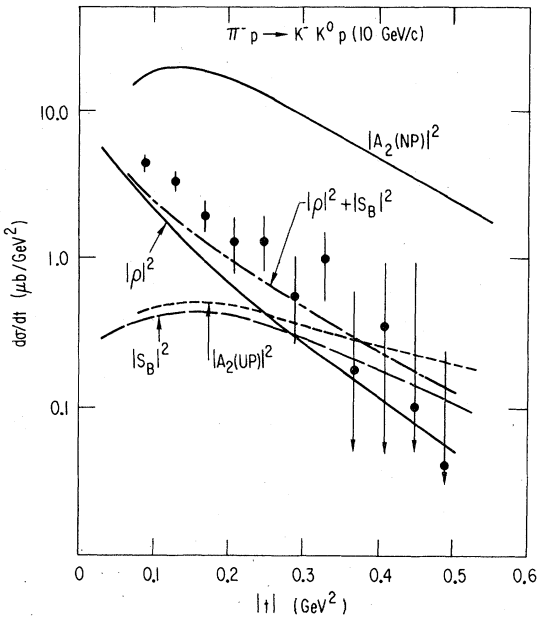

FIG. 24. Momentum-transfer dependence of the large wave in $\pi^-p \to K^-K^0p$ from Ref. 28, together with cross sections for $I=1$ S and P waves ($|S_B|^2$ and $|\rho|^2$, respectively) predicted from our K^-K^+ analysis. For comparison, the $A_2(1310)$ cross sections from Ref. 16 are shown for the unnatural (dotted curve) and natural (solid curve) parity projections.

t dependence of the large wave. (4) The NPE production cross section for A_2^- in reaction (4) (top solid curve) has a t dependence which is similar to the large wave within errors.

Thus, a skeptical interpretation of the large wave would be that it reflects the ρ^- and S_B contributions which are certainly present, plus feedthrough from the A_2^- NPE cross section; the latter could account for the enhancement in the large wave near 1300 MeV.

Taking the data at face value, Martin and Ozmutlu[16] assumed that the large wave is in fact the $I=1$ S wave, and ascribed its steep t dependence to a dominant Z-exchange mechanism.[29] Using their $I=1$ S wave (S_Z) as input, they reanalyzed the 6-GeV/c K^-K^+ data and found that some of the enhancement in the 1300-MeV region in our solution I(b) could be attributed to S_Z.

We have likewise repeated our amplitude analysis of the 6-GeV/c K^-K^+ data as a function of $\overline{K}K$ mass in order to see what effect a large S_Z wave would have on the determination of the $S_{I=0}$ (S_π) and $S_{I=1}$ (S_B) waves of solution I(b). We have also extended this analysis to the larger-t region, $0.08 < |t| < 0.20$ GeV^2, where we might hope to see the hypothetical $I=1$ resonance in S_B as well as in S_Z; S_B increases with t relative to S_π, and should be better measured at larger t (cf. Fig. 20). In this

analysis we parametrized the S_Z contribution as a Breit-Wigner resonance, normalized to agree in magnitude with the large wave at 1300-MeV K^-K^0 mass (as in Fig. 23); S_Z was extrapolated from 10 to 6 GeV/c using a p_{lab}^{-1} amplitude dependence. For simplicity, the P and D waves were parametrized with smooth resonance contributions from ρ, ω, f, f', and A_2^0; the t dependences and production phases of these waves were based on the properties of solution I(b) discussed above, and on analyses of A_2^0 production in the $(\bar{K}K)$ (Ref. 28) and (3π) (Ref. 22) channels. We assumed that S_Z does not interfere with S_π or S_B or with the P- or D-wave amplitudes. While it is possible that the ω tail ($P_{I=0}$) and the A_2^0 wave ($D_{I=1}$) have some Z-exchange component, the striking difference in t dependence between these waves and S_Z, as shown in Fig. 24, suggests that the ω and A_2^0 waves are dominated by B exchange. In any case, the ω and A_2^0 waves are small, and the dominant OPEA waves ($P_{I=1}$ and $D_{I=0}$) cannot interfere with S_Z. As a result, $|S_Z|^2$ must contribute incoherently to the S waves in both reactions (1) and (2), thus mimicking the effect of the $I=0$ S wave. Furthermore, the observation of large SP and SD interference moments places a natural restriction on the allowable amount of S_Z.

Figure 25 shows the solutions for $|S_{I=0}|$ and $|S_{I=1}|$ in the two t intervals. The solid points represent the S-wave magnitudes with S_Z set to zero; the open points show the $|S_{I=0}|$ values when S_Z is constrained according to our extrapolation of the K^-K^0 large wave (depicted by the solid curve in Fig. 25). As expected, only $|S_{I=0}|$ is affected by the inclusion of S_Z; $|S_{I=1}|$ and the S-wave phases are independent of S_Z, within errors. The phases found for $S_{I=0}$ and $S_{I=1}$ are shown in Fig. 26, where the two t regions are compared. Several conclusions can be drawn. (1) Some of the enhancement in $S_{I=0}$ at 1300 MeV can be absorbed in the S_Z contribution [Figs. 25(a) and 25(b)]. However, a strong shoulder persists in $|S_{I=0}|$ around 1300 MeV, regardless of the choice of S_Z. (2) Even at larger t [Fig. 25(d)], there is no evidence for any clear resonance structure at 1300 MeV in $|S_B|$; moreover, S_B [Fig. 26(b)] does not display any Breit-Wigner phase variation. (3) The $S_{I=0}$ phase [Fig. 26(a)] is identical in the two t regions, within errors. Thus, aside from the modest slope-mass correlation discussed in the previous section, there is no evidence that the $S_{I=0}$ production mechanism (as exemplified by its t dependence) changes in the 1300 MeV mass region. (4) Finally, we note that the S_Z wave shown in Fig. 25 is relatively large; as might be expected, inclusion of this S_Z contribution results in decreased coherence between the S wave and the P and D waves, and gives significantly poorer fits.

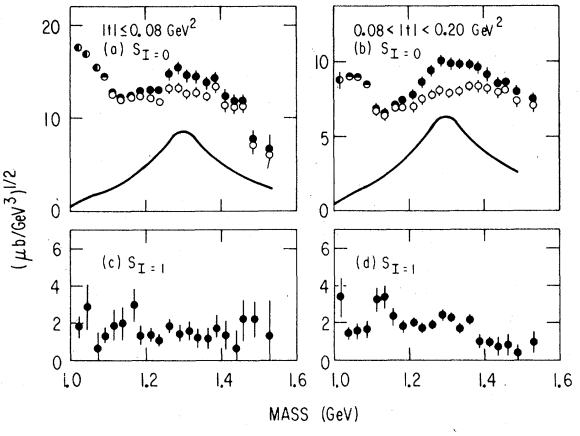

FIG. 25. Magnitudes of $|S_{I=0}|$, (a) for $|t|<0.08$ GeV^2, (b) for $0.08<|t|<0.20$ GeV^2; magnitudes of $|S_{I=1}|$, (c) for $|t|<0.08$ GeV^2, (d) for $0.08<|t|<0.20$ GeV^2. The open points show $|S_{I=0}|$ with an additional S_Z resonance, shown by the solid curves, input in the fit; the solid points are the amplitudes with S_Z constrained to zero. The fits used the 6-GeV/c data from reactions (1) and (2), with smooth parametrizations of the P and D waves.

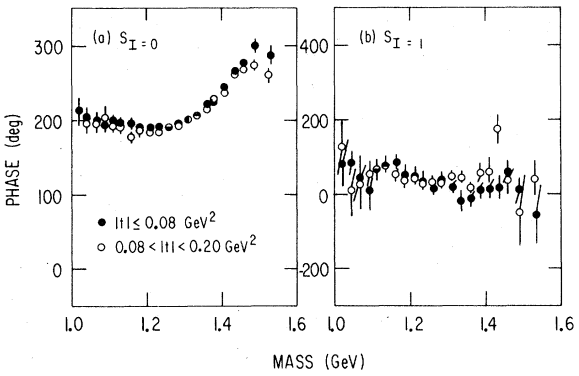

FIG. 26. Phases of (a) $S_{I=0}$ and (b) $S_{I=1}$ as functions of K^-K^+ mass. The solid points denote $|t|<0.08$ GeV^2, the open points $0.08<|t|<0.20$ GeV^2. These fits used smooth parametrizations of the P and D waves, and S_Z was constrained to zero.

To summarize, we cannot exclude the possibility of an $I=1$ S-wave resonance at 1300 MeV produced by Z exchange, as hypothesized by Martin and Ozmutlu.[16] However, the only evidence for such a resonance comes from the rather marginal enhancement seen in the K^-K^0 large wave in Fig. 23; we have suggested that this enhancement might reflect feedthrough from the dominant A_2-resonance contribution in this channel. There is no indication of Breit-Wigner behavior in the $I=1$ B-exchange S wave in K^-K^+, even at larger t where S_B is more prominent. Moreover, inclusion

of an S_Z resonance does not affect the amplitudes of solution I(b) in any way except to reduce the 1300-MeV enhancement in $S_{I=0}$ by $\lesssim 15\%$. Thus, the interpretation of the dominant $\bar{K}K$ S-wave amplitudes does not depend critically on our assumptions regarding Z exchange.

VI. INTERPRETATION OF THE $I=0$ S WAVE

The physical effects which are prominent in the $I=0$ $\bar{K}K$ S wave, namely the $S^*(980)$ threshold effect and the broad enhancement at 1300 MeV, also occur in $\pi\pi$ elastic scattering, and one cannot hope to understand the behavior of the $\pi\pi \to \bar{K}K$ amplitude without taking into account the unitarity constraints on the coupled-channel S matrix. The relevant constraints are derived in the Appendix to this paper. A popular approach has been to fit the $\pi\pi \to \pi\pi$ and $\pi\pi \to \bar{K}K$ data with a unitary K-matrix parametrization, and search the resultant T matrix for Breit-Wigner poles in the complex energy plane.[30] Estabrooks[9] reported such an analysis, using our data, in which the K matrix was parametrized as a sum of poles associated with $\epsilon(\sim 800)$, $S^*(\sim 980)$, and $\epsilon(\sim 1500)$ resonances. Martin and Ozmutlu[16] analyzed the same data with the inverse K matrix parametrized as a smooth polynomial, but did not find Breit-Wigner T-matrix poles. We have repeated these exercises, with similar results. We find that a K-matrix parametrization with simple poles [cf. Eq. (A6)] does not give good quantitative fits to the data, the reasons for which are explained in the Appendix. On the other hand, the polynomial K^{-1} matrix gives a good description in the physical region, but does not extrapolate stably into the complex plane. Thus, we have been led to a somewhat different approach: We have tried to understand the physical features of the observed T matrix directly in terms of resonant and nonresonant components constrained by unitarity.

We have extracted the $\pi\pi \to \bar{K}K$ scattering amplitude from solution I(b) using the extrapolation

$$S_{I=0} = \frac{C}{p_{\text{lab}}} \frac{\sqrt{-t}}{\mu^2 - t} \exp[B_S(t-\mu^2)] \frac{M}{\sqrt{q_\pi}} \frac{2T(\pi\pi \to \bar{K}K)}{\sqrt{3}}, \tag{12}$$

where $|T(\pi\pi \to \bar{K}K)| \leq \frac{1}{2}$ is the unitarity limit. We have chosen $C = 3.6$ mb$^{1/2}$ as found in S-wave dipion production,[12] and B_S consistent with Fig. 21; we note that, if anything, $T(\pi\pi \to \bar{K}K)$ may be underestimated with this choice of C. The resulting magnitude $|T(\pi\pi \to \bar{K}K)|$ is shown in Fig. 27; the phase of $T(\pi\pi \to \bar{K}K)$, denoted $\phi(\pi\pi \to \bar{K}K)$, is simply the small-$t$ $I=0$ S-wave phase shown in Fig. 26(a).

The 1300-MeV bump in the $I=0$ S wave shows up as a broad enhancement in $|T(\pi\pi \to \bar{K}K)|$, followed by a rapid dropoff above 1400 MeV. The phase $\phi(\pi\pi \to \bar{K}K)$ is stationary over the lower half of the bump, but rises rapidly above 1300 MeV. Using a smooth inverse-K-matrix parametrization of $T(\pi\pi \to \bar{K}K)$, we obtain the Argand plot shown in Fig. 28(a). This plot indicates a Breit-Wigner

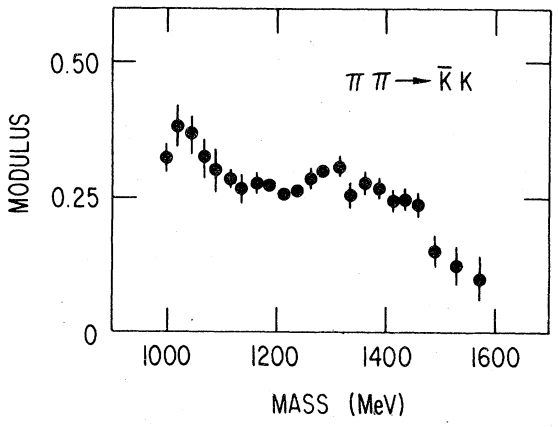

FIG. 27. Modulus of the $\pi\pi \to \bar{K}K$ scattering amplitude $|T(\pi\pi \to \bar{K}K)|$ from solution I(b).

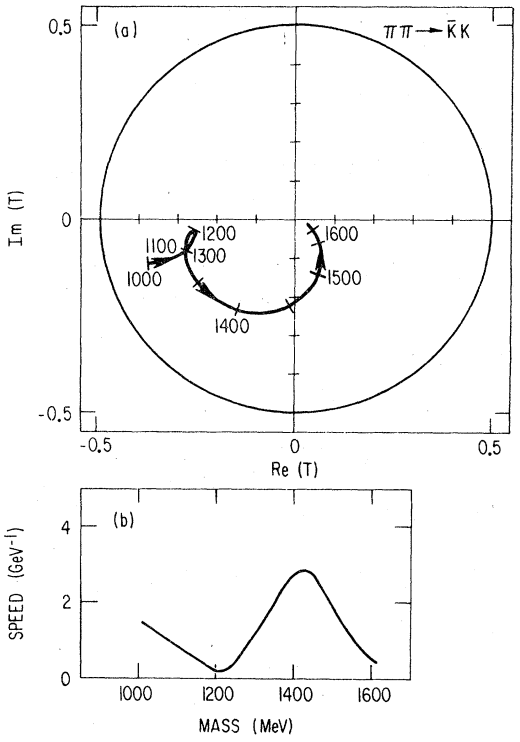

FIG. 28. (a) Argand-plot representation of $T(\pi\pi \to \bar{K}K)$, and (b) speed $|dT(\pi\pi \to \bar{K}K)/dM|$.

resonance loop, centered around 1425 MeV, superimposed on a very large background amplitude; the background, which is generated by the $S^*(980)$ effect, has a ~190° phase and diminishes slowly with increasing mass. Figure 28(b) shows the speed, $|dT/dM|$, for $T(\pi\pi \to \bar{K}K)$. For a Breit-Wigner resonance on a slowly varying background, it is easily shown that $|dT/dM|$ is proportional to the Breit-Wigner intensity. Thus, the speed measurement indicates a resonance at $M_R \sim 1425$ MeV with $\Gamma \sim 160$ MeV. From the diameter of the loop in the Argand plot, we can also infer the relative coupling of this object to $\pi\pi$ and $\bar{K}K$, namely $(x_\pi x_K)^{1/2} \approx 0.3$ to 0.4, where $x_i = \Gamma_i/\Gamma$. This range of couplings is equivalent to $0.8 \leq x \leq 0.9$, x being the larger of the two branching ratios, implying that the resonance couples asymmetrically to the two channels; as discussed below, the $\pi\pi$ phase shifts suggest that it is the $\pi\pi$ rather than the $\bar{K}K$ channel which has the larger coupling. We will henceforth refer to this object as $\epsilon(1425)$.

In principle, the $IJ^{PC} = 00^{++}$ system can communicate with channels other than $\pi\pi$ and $\bar{K}K$, in particular $\eta\eta$, $\rho\rho$, $\omega\omega$, and πA_1. Unfortunately, only the $\pi\pi$ and $\bar{K}K$ channels have been measured. It is plausible that the $\rho\rho$, $\omega\omega$, and πA_1 channels are inhibited below 1500 MeV by limited phase space, and in the case of πA_1, orbital momentum barrier effects. As for the $\eta\eta$ channel, there is no evidence for any drastic effects near $\eta\eta$ threshold in either $\pi\pi \to \pi\pi$ or $\pi\pi \to \bar{K}K$, in contrast to the strong influence of the $\bar{K}K$ threshold on $\pi\pi \to \pi\pi$. We also note that the SU(3) widths for an ϵ-like state (i.e., a $\bar{u}u + \bar{d}d$ quark configuration) would be 27 : 9 : 1 for the $\pi\pi : \bar{K}K : \eta\eta$ channels, while for an $\bar{s}s$ quark state, these ratios would be 0 : 9 : 4, assuming the Okubo-Zweig-Iizuka (OZI) rule. Thus, there is some phenomenological justification for ignoring all but the $\pi\pi$ and $\bar{K}K$ channels, at least below 1500 MeV.

The two-channel T matrix can be specified with three independent parameters. Two of these, the elasticity η and the sum of the $\pi\pi$ and $\bar{K}K$ elastic phase shifts $\delta_\pi + \delta_K$, can be extracted from the amplitude $T(\pi\pi \to \bar{K}K)$ [cf. Eq. (A1)]. The $\pi\pi$ phase-shift analyses[31-33] provide the third parameter δ_π. Measurements of the elasticity in $\pi\pi \to \pi\pi$ are redundant, and aside from consistency checks, we have used $\pi\pi \to \bar{K}K$ to determine η. In contrast with our unique solution for $\pi\pi \to \bar{K}K$, eight discrete solutions for the $\pi\pi$ phase shifts have been obtained in the 1000–1600 MeV mass region. Two representative solutions, A and B from Ref. 31, are shown as smooth interpolations in Fig. 29(a); the other six solutions are variants of A and B. Refinements of the A and B solutions known as α, β, and β' were obtained by Pennington and Martin,[33] and their solution β is displayed also in Fig. 29(a). A recent analysis of dipion production from a polarized proton target, taking into account the overall behavior of the S, P, and D waves, strongly suggests that the correct solution must be close to β and β', rather than A, B, or α.[34] Figure 29(a) shows the "unique" phase shifts extracted from the polarized target data of Ref. 34, and Fig. 30 compares the modulus of the $\pi\pi \to \pi\pi$ S wave with the predictions of solutions A, B, and β using our determination of the elasticity η.[35] We see that solution β gives a satisfactory description of the polarized-target data, while the slow variation of solution A can be ruled out above 1400 MeV.

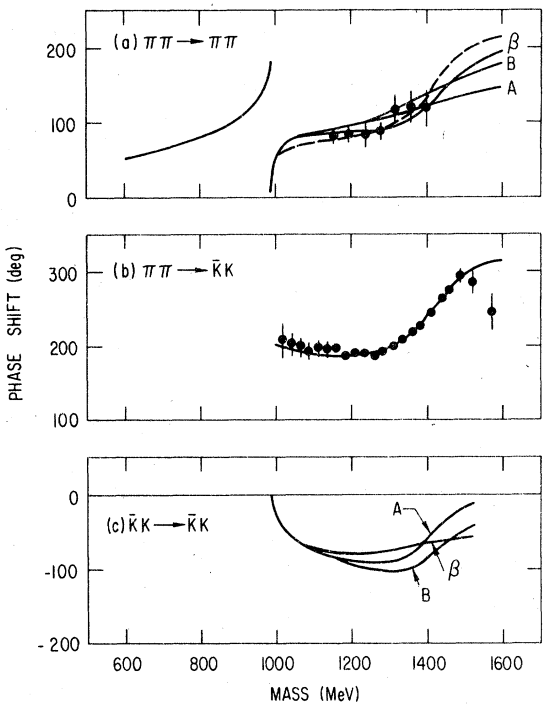

FIG. 29. (a) Smooth interpolations of measured $\pi\pi$ elastic phase shifts from solutions A and B of Ref. 32 and β of Ref. 33; the dashed curve shows the phase shifts predicted from our fit to $\phi(\pi\pi \to \bar{K}K)$ with $x_\pi = 0.85$. (b) The measured phases, $\phi(\pi\pi \to \bar{K}K)$, together with results of our fit. (c) Smooth interpolation of the $\bar{K}K$ elastic phase shifts, obtained from the $\pi\pi$ phase shifts and $\phi(\pi\pi \to \bar{K}K)$.

Comparison of Figs. 29(a) and 29(b) shows that the $\epsilon(1425)$ produces quite similar acceleration in both δ_π (solution β) and $\phi(\pi\pi \to \bar{K}K)$ above 1300 MeV, implying that the $\epsilon(1425)$ affects mainly δ_π, not δ_K [note that $\phi(\pi\pi \to \bar{K}K) = \delta_\pi + \delta_K$]. Figure 29(c) shows the $\bar{K}K \to \bar{K}K$ elastic phase shift δ_K obtained by subtracting δ_π from $\phi(\pi\pi \to \bar{K}K)$. For solution β, δ_K varies little with mass except for the rapid excursion near threshold, and does not

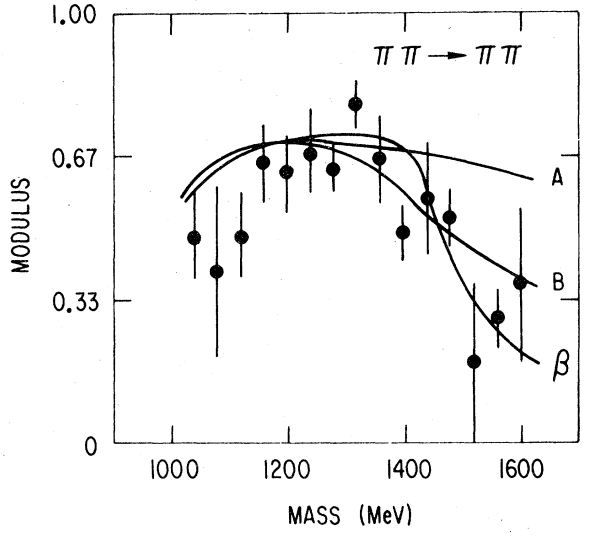

FIG. 30. Modulus of the $\pi\pi \rightarrow \pi\pi$ S-wave amplitude (defined as $\frac{2}{3}T(I=0)+\frac{1}{3}T(I=2)$, from Ref. 34; the curves A, B, and β are predictions using the $\pi\pi$ phase shifts of Refs. 32 and 33 and elasticity measured in $\pi\pi \rightarrow \overline{K}K$.

show any $\epsilon(1425)$ effect; the slowly varying A- and B-type phase shifts yield more variation in δ_K. It is noteworthy that both the β and B $\pi\pi$ phase-shift solutions, irrespective of speed, exhibit an overall phase advance of $\approx 100^\circ$ in the 1200–1600 MeV region, similar to the $\approx 100^\circ$ advance found in $\phi(\pi\pi \rightarrow \overline{K}K)$; for both solutions, this advance in δ_π is accompanied by a net change of $\approx 0^\circ$ in δ_K. Thus, while the speed behavior of solution β needs confirmation, the measured phases naturally suggest a predominantly $\pi\pi$ coupling for the $\epsilon(1425)$.

The phase $\phi(\pi\pi \rightarrow \overline{K}K)$ alone is sufficient to determine the $\epsilon(1425)$ mass and width. If we decompose the T matrix into a resonance contribution T^R and a unitary background T^B,

$$T = T^B + T^R , \tag{13}$$

then unitarity provides the relation

$$\phi(\pi\pi \rightarrow \overline{K}K) = \delta^R + \delta_\pi^B + \delta_K^B , \tag{14}$$

where δ_π^B and δ_K^B are the background phase shifts associated with T^B, and δ^R is the phase that would apply to a background-free Breit-Wigner resonance, namely $\delta^R = \arg(M_R - M + i\Gamma/2)$ [cf. Eqs. (A14) and (A15)]. Using a smooth parametrization of the background phase shifts, as discussed below, we have fitted $\phi(\pi\pi \rightarrow \overline{K}K)$ to obtain $M_R = 1425 \pm 15$ MeV and $\Gamma = 160 \pm 30$ MeV; this fit is shown by the curve in Fig. 29(b). We can also predict the $\pi\pi$ phase shifts from this fit. For a predominantly $\pi\pi$ coupling, the $\pi\pi$ phase shift is equal to the quantity $\delta^R + \delta_\pi^B$ within a small deviation which depends on x_π [cf. Eq. (A19a)]. The dashed curve in Fig. 29(a) shows the prediction for $x_\pi = 0.85$. We emphasize that this curve, which is similar to solution β, is derived from $\phi(\pi\pi \rightarrow \overline{K}K)$ and is not the result of a fit to the $\pi\pi$ data. The curves overshoot both of the measured phases $\phi(\pi\pi \rightarrow \overline{K}K)$ and δ_π at high masses; however, this is a region in which both $T(\pi\pi \rightarrow \pi\pi)$ and $T(\pi\pi \rightarrow \overline{K}K)$ are small in magnitude, and the other neglected channels (e.g., $\rho\rho$, $\omega\omega$, πA_1) may be growing in importance.

A consistency check on our analysis is provided by the K matrix. Rather than fit the T matrix in terms of a K-matrix parametrization, we can in fact determine the K-matrix elements at each mass from the measured T-matrix parameters η, δ_π, and δ_K. The result for the quantity $\mathrm{Det}(K^{-1})$ is shown in Fig. 31. This determinant must vanish at the location of a K-matrix pole, and we find that all $\pi\pi$ phase-shift solutions require such a pole near 1400 MeV. This K-matrix pole is clearly associated with the $\epsilon(1425)$, and the absence of other zeros in Fig. 31 suggests that the $\epsilon(1425)$ is the only $I=0$ S-wave resonance in the 1000–1500 MeV mass region.

We now turn to consideration of the background under the $\epsilon(1425)$ resonance, since some qualitative understanding of this background is needed to explain the intensity patterns in the observed T

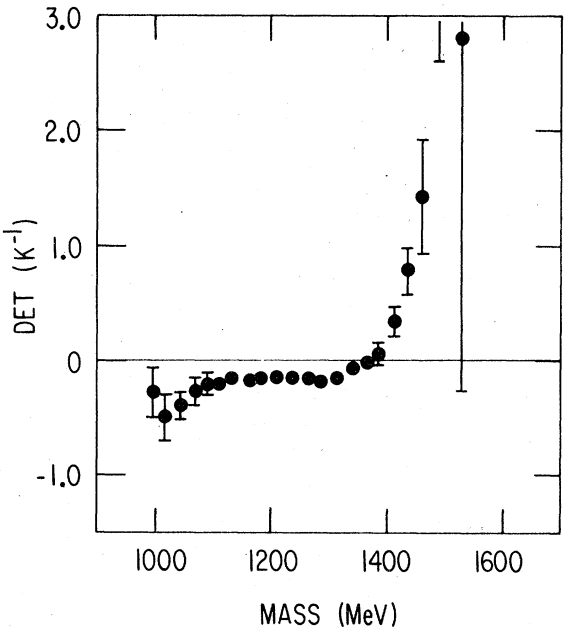

FIG. 31. Determinant of the inverse K matrix for $\pi\pi$ solution β, using measured $T(\pi\pi \rightarrow \overline{K}K)$ and $\pi\pi \rightarrow \pi\pi$ elastic phase shifts as input. Other $\pi\pi$ solutions give similar behavior.

matrix. In addition, the nature of the S^* effect is of interest in its own right. We first recall that in Morgan's model of the $\pi\pi \to \pi\pi$ amplitude,[8] three ingredients were needed to explain the $\pi\pi$ phase shifts, namely an $S^*(980)$ Breit-Wigner resonance, an $\epsilon(\approx 1300)$ resonance, and a constant background phase shift, $\delta_\pi^0 \approx 30°$. The $S^*(980)$, with a width of order 200 to 300 MeV, accounted for the 180° phase advance of δ_π in the region 900–1100 MeV [cf. Fig. 29(a)], while the very broad $\epsilon(\approx 1300)$ accounted for the $\approx 100°$ phase advance of the A- and B-type solutions between 1200 and 1600 MeV. The background phase shift δ_π^0 was needed to explain the large $\pi\pi$ phase shift observed in the $\rho(770)$ region. The combination of δ_π^0 with the $\epsilon(\approx 1300)$ tail caused the $\pi\pi$ amplitude to sit near the top of the Argand plot in this region, and explained the fact that the S^* causes a dip, rather than a peak, in the $\pi\pi$ intensity. (The S^* drives the $\pi\pi$ amplitude to the bottom of the Argand plot.)

If we replace Morgan's $\epsilon(\approx 1300)$ with the narrower $\epsilon(1425)$, then the same picture can still explain the $\pi\pi$ phase shifts, provided that the background phase shift δ_π^0 is increased to around 60° [the $\epsilon(1425)$ is too narrow to build up δ_π in the $\rho(770)$ region]. However, in extending this description to the $\bar{K}K$ channel, care must be taken in parametrizing the S^* effect. The S^* clearly acts like a relatively narrow ($\Gamma_\pi^S \approx 200$ MeV) Breit-Wigner resonance in $\pi\pi \to \pi\pi$, below $\bar{K}K$ threshold. However, if the S^* is a Breit-Wigner resonance, its width must be very large above $\bar{K}K$ threshold. Using the same arguments that we have applied to the $\epsilon(1425)$, the $\pi\pi \to \bar{K}K$ phase is given by $\phi(\pi\pi \to \bar{K}K) = \delta^S + \delta_\pi^0$ in the threshold region, where δ^S is the S^* Breit-Wigner phase [$\delta^S = \arg(M_S - M + i\Gamma_S)$]. Since $\phi(\pi\pi \to \bar{K}K)$ is constant or slowly falling above $\bar{K}K$ threshold [Fig. 29(b)], we conclude that δ^S is stationary and that Γ_S must be much larger than $M_S - M$ for $M \lesssim 1300$ MeV (i.e., Γ_S is effectively hundreds of MeV).[36] This inconsistency of $\phi(\pi\pi \to \bar{K}K)$ with narrow Breit-Wigner behavior was noted by Martin and Ozmutlu.[16] If the S^* is regarded as a very broad resonance, then the rapid excursion of the $\bar{K}K$ elastic phase shift to $-90°$ in Fig. 29(c) can be viewed as a consequence of the very rapid increase in $\Gamma(S^* \to \bar{K}K)$ above $\bar{K}K$ threshold. Specifically, the elastic $\bar{K}K$ amplitude defined by

$$T(\bar{K}K \to \bar{K}K) = \frac{\Gamma_K^S/2}{M_S - M - i(\Gamma_\pi^S + \Gamma_K^S)/2} \qquad (15a)$$

jumps to the top of the Argand plot as Γ_K^S increases, tracing out a negative phase shift for $M > M_S$; the overall phase of $T(\bar{K}K \to \bar{K}K)$, as distinct from the phase shift, is given by δ^S and is essentially constant. One difficulty with this representation in terms of a very broad Breit-Wigner resonance is that the amplitude for $\pi\pi \to \bar{K}K$,

$$T(\pi\pi \to \bar{K}K) = \frac{(\Gamma_\pi^S \Gamma_K^S/2)^{1/2}}{M_S - M - i(\Gamma_\pi^S + \Gamma_K^S)/2}, \qquad (15b)$$

should approach the unitarity limit $|T(\pi\pi \to \bar{K}K)| \approx 0.5$ at a mass where $\Gamma_\pi^S = \Gamma_K^S$; however, the observed maximum value is $|T(\pi\pi \to \bar{K}K)| \leq 0.4$ (Fig. 27).

An alternative description of the S^* which better matches the data is in terms of a $\bar{K}K$ virtual bound state. The parametrization we have chosen is equivalent to a pole-free K matrix with strong coupling between $\pi\pi$ and $\bar{K}K$, namely

$$S^B(\pi\pi \to \pi\pi) = \frac{-q_R^* - q_K}{q_R - q_K} e^{2i\delta_\pi^0}, \qquad (16a)$$

$$S^B(\bar{K}K \to \bar{K}K) = \frac{q_R + q_K}{q_R - q_K}, \qquad (16b)$$

where $q_K \to i|q_K|$ below $\bar{K}K$ threshold, and q_R defines the complex position of a sheet-II pole in the S matrix. The expressions for δ_π^0 and q_R in terms of the three K-matrix elements are given in Ref. 8. In our fit to $\phi(\pi\pi \to \bar{K}K)$ we have used $\delta_\pi^0 \sim 60°$ and $q_R \sim -0.06 + 0.14i$ (GeV); the background phase shifts, δ_π^B and δ_K^B in Eq. (14), are sensitive mainly to δ_π^0 and $\mathrm{Im}(q_R)$. Similar constant-K-matrix parametrizations have been used by other authors to describe the S^* effect in $\pi\pi \to \pi\pi$.[37] We emphasize that the S^B matrix in Eq. (16) has only a single sheet-II pole, which induces Breit-Wigner behavior in $\pi\pi \to \pi\pi$ below $\bar{K}K$ threshold. This parametrization describes the behavior of $\phi(\pi\pi \to \bar{K}K)$ and δ_K in a natural way, and does not require $|T(\pi\pi \to \bar{K}K)|$ to reach the unitarity limit above $\bar{K}K$ threshold.

The physical quantities which are not determined by the fit to $\phi(\pi\pi \to \bar{K}K)$, but appear instead in the modulus $|T(\pi\pi \to \bar{K}K)|$, are the $\epsilon(1425)$ relative coupling $(x_\pi x_K)^{1/2}$ and the S^* background intensity; the latter is mainly sensitive to $\mathrm{Re}(q_R)$ in Eq. (16). Specifically, the moduli for $T(\pi\pi \to \bar{K}K)$ and for the background and resonance components T^B and T^R can be expressed in terms of the Breit-Wigner phase δ^R [known from the fit to $\phi(\pi\pi \to \bar{K}K)$] and the coupling $(x_\pi x_K)^{1/2}$ as follows [cf. Eqs. (A14)]:

$$|T(\pi\pi \to \bar{K}K)| = (x_\pi x_K)^{1/2} |\sin(\delta^R + \theta)|, \qquad (17a)$$

$$|T^B(\pi\pi \to \bar{K}K)| = (x_\pi x_K)^{1/2} \sin\theta, \qquad (17b)$$

$$|T^R(\pi\pi \to \bar{K}K)| = (x_\pi x_K)^{1/2} \sin\delta^R. \qquad (17c)$$

The unitarity phase in Eqs. (17), θ $(=\theta_\pi + \theta_K)$, parametrically links the measured intensity with the S^* background intensity. Note that the background phase shifts do not enter the intensity expressions at all. Figure 32 displays the geometrical relation between the components T, T^B, and T^R for the $\pi\pi \to \bar{K}K$ amplitudes.

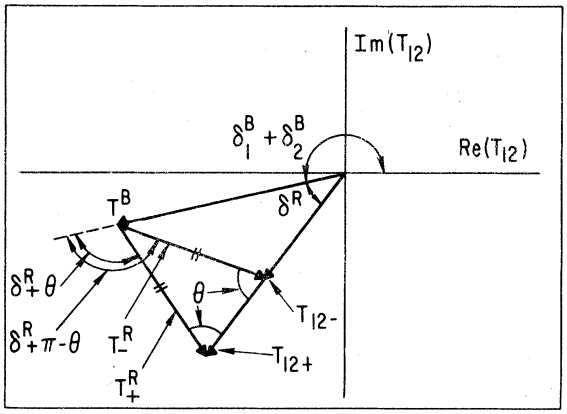

FIG. 32. Decomposition of the cross-channel amplitude T_{12} for a two-channel T matrix, into resonance contribution T_{12}^R, and background T_{12}^B, corresponding to the unitary solutions of Eq. (A7). For fixed $|T_{12}^B|$, there are two solutions (T_{12+} and T_{12-}) for T_{12}, which correspond to the unitarity phases θ and $\pi-\theta$ ($\theta=\theta_1+\theta_2$) assigned to the T_{12}^R contribution. The resonance phase δ^R is given by $\mathrm{Arg}[M_R-M+i\Gamma_R/2]$ and $\delta_1^B+\delta_2^B$ is the background phase.

The broad enhancement at 1300 MeV in $\pi\pi\to\bar{K}K$ (see Fig. 27) can now be understood as a shift of the $\epsilon(1425)$ peak caused by the large background. For zero background, we would have $\theta=0$ [cf. Eq. (17b)] and $T(\pi\pi\to\bar{K}K)$ would peak at $\delta^R=90°$ from Eq. (17a), as expected for a pure Breit-Wigner resonance. However, for nonzero background θ is positive, and in general the combination $\theta+\delta^R$ goes through 90° at lower mass, generating the maximum in $|T(\pi\pi\to\bar{K}K)|$. Note that if θ and $|T^B|$ fall with mass, as expected for the S^* background, then the combination $\theta+\delta^R$ tends to remain stationary, leading to an enhancement which is broader than the $\epsilon(1425)$ width.

These considerations are illustrated in Fig. 33. Lacking a unique prescription for the background intensity, we have considered a range of solutions for $|T^B|$ and $(x_\pi x_K)^{1/2}$, using the parametrization of Eq. (16) and allowing $\mathrm{Re}(q_R)$ to have a linear mass dependence. Figure 33(a) shows a typical solution for the contributions of $|T^R|$ and $|T^B|$ to $|T(\pi\pi\to\bar{K}K)|$; the measured values of $(x_\pi x_K)^{1/2}$ for this choice of $|T^B|$ are plotted in Fig. 33(b). Figure 33(c) shows the angles θ and δ^R. The combination $\theta+\delta^R$ goes through a broad minimum around 1300 MeV, generating the maximum in $|T(\pi\pi\to\bar{K}K)|$. The mass dependence of $|T(\pi\pi\to\bar{K}K)|$ owes as much to the variation of θ as it does to the Breit-Wigner behavior of δ^R, and consequently the shape of the 1300-MeV enhancement is not well correlated with the properties of the $\epsilon(1425)$. Given the uncertainty in $|T^B|$, we can only place limits on the relative coupling $0.28\leq(x_\pi x_K)^{1/2}\leq 0.40$. Note that the lower limit is dictated by unitarity, since $|T(\pi\pi\to\bar{K}K)|\leq(x_\pi x_K)^{1/2}$ must be satisfied, at least in the vicinity of the resonance [cf.

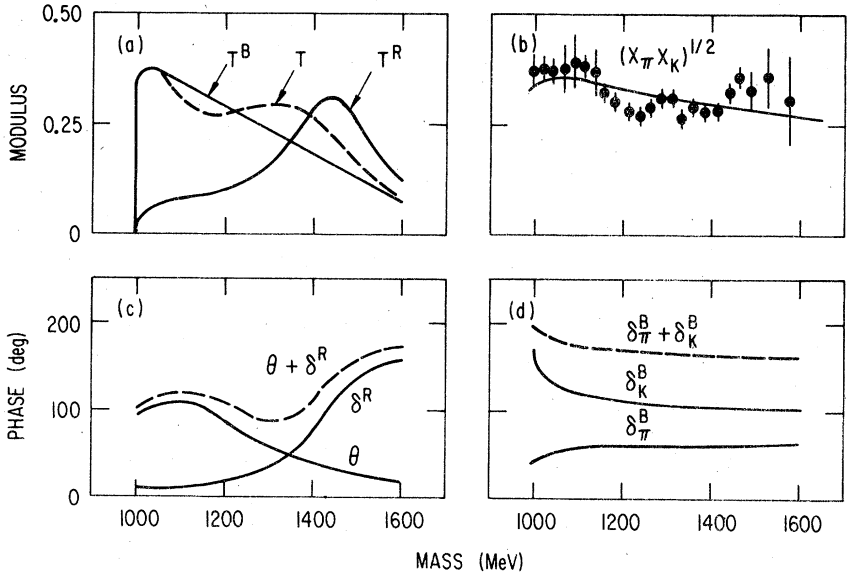

FIG. 33. (a) Moduli of the amplitudes $T(\pi\pi\to\bar{K}K)$, $T^B(\pi\pi\to\bar{K}K)$, and $T^R(\pi\pi\to\bar{K}K)$ for a typical parametrization of the background T^B; (b) coupling of the $\epsilon(1425)$, $(x_\pi x_K)^{1/2}$ obtained from measured values of $|T(\pi\pi\to\bar{K}K)|$ for the same background as in (a); the curve shows the behavior expected for a constant coupling using the formalism of Ref. 38; (c) unitarity phase $\theta=\theta_\pi+\theta_K$, and Breit-Wigner phase δ^R for amplitudes shown in (a), together with $\theta+\delta^R$; (d) background phase shifts δ_π^B and δ_K^B, from the fit to Eq. (16), together with $\delta_\pi^B+\delta_K^B=\mathrm{Arg}(T_{12}^B(\pi\pi\to\bar{K}K))$.

Eq. (17a)].

As noted in the Appendix, there is a discrete ambiguity in the solutions for the unitarity phase, corresponding to the possible solutions $\delta^R+\theta$ and $\pi-\delta^R-\theta$ for Eq. (17a); the quadrant choice affects the value of $|T^B(\pi\pi\to\bar{K}K)|$ [Eq. (17b)]. For reasonable values of $(x_\pi x_K)^{1/2}$, one of these solutions requires $T^B(\pi\pi\to\bar{K}K)$ to go through the origin around 1300 MeV, and this can be dismissed as unphysical. The solutions which survive have θ in the range $0\leq\theta\leq\pi/2$, and as discussed in the Appendix, this implies a positive relative coupling of $\epsilon(1425)$ to $\pi\pi$ and $\bar{K}K$.

One unattractive feature of our solution is that the coupling $(x_\pi x_K)^{1/2}$ falls with mass, whereas for $x_\pi \gg x_K$, we would expect the opposite behavior. However, the increase of $(x_\pi x_K)^{1/2}$ near threshold is a unitarity requirement [$(x_\pi x_K)^{1/2}\geq|T^B(\pi\pi\to\bar{K}K)|$], and it is in general not possible to insist on phase-space-behaved widths in the presence of a large background. As noted in the Appendix, simple K-matrix parametrizations of the $\epsilon(1425)$ would require even more complicated and apparently unphysical behavior for the partial widths. Novoseller[38] has suggested a modification to the formalism that we have adopted, in which the resonance couplings are redefined by a unitary transformation which makes them independent of the background parametrization (see the Appendix). The curve in Fig. 33(b) shows the mass dependence expected for $(x_\pi x_K)^{1/2}$, using a constant relative coupling $(x'_\pi x'_K)^{1/2}=0.24$, where x'_π, x'_K refer to the partial widths as defined in the Novoseller scheme. The observed increase of $(x_\pi x_K)^{1/2}$ near threshold is explained at least qualitatively.

The prediction for the intensity in $\pi\pi\to\pi\pi$ is straightforward and is essentially identical with that for solution β, indicated in Fig. 30. As in $\pi\pi\to\bar{K}K$, the intensity peak in $\pi\pi\to\pi\pi$ occurs below the $\epsilon(1425)$ resonance. Like the S^* effect, the $\epsilon(1425)$ sits on a large background ($\delta^B_\pi\approx 60°$), and consequently drives the $\pi\pi$ amplitude to the bottom of the Argand plot, causing an intensity minimum around 1500 MeV. We note that the $K\pi$ S-wave phase shifts[39] behave in an analogous fashion, with an increased speed above 1400 MeV and an intensity minimum at $\approx$1600 MeV. Thus we surmise that the $\epsilon(1425)$ and the $\kappa(\approx 1500)$ (Ref. 9) are related phenomena (i.e., members of the same scalar nonet) while the strong background amplitudes may be four-quark phenomena as discussed in Refs. 10 and 11. In particular, the interpretation of the S^* as a $\bar{K}K$ bound state suggests that the S^* is not a simple $Q\bar{Q}$ system.

To summarize the properties of the $\epsilon(1425)$, we have obtained $M=1425\pm 15$ MeV, $\Gamma=160\pm 30$ MeV, and $0.28\leq(x_\pi x_K)^{1/2}\leq 0.40$, with a positive relative coupling for $\pi\pi$ and $\bar{K}K$. The magnitude of the coupling is uncertain because it is strongly correlated with the background intensity, which can be constrained only by smoothness requirements. We have hypothesized that the coupling is mainly to $\pi\pi$ ($x_\pi\approx 0.85$), but this requires confirmation of the speed pattern observed in solution β for $\pi\pi\to\pi\pi$. Assuming the OZI rule, a nonstrange $I=0$ $Q\bar{Q}$ state (i.e., $\bar{u}u+\bar{d}d$) with phase-space-behaved widths would have a coupling $(x_\pi x_K)^{1/2}\approx 0.40$, while a pure SU(3) singlet such as a glueball would have $(x_\pi x_K)^{1/2}\approx 0.50$; the latter is certainly incompatible with the data.

VII. SUMMARY

We have carried out an amplitude analysis of the K^-K^+ system produced in the reactions $\pi^-p\to K^-K^+n$ and $\pi^+n\to K^-K^+p$ at 6 GeV/c. The data were obtained in a high-statistics experiment using the Argone effective-mass spectrometer. Combining the results from the two reactions has allowed us to separate the $\bar{K}K$ production amplitudes into their $I=0$ and $I=1$ components.

Starting with coherence assumptions based on absorbed pion exchange, we have obtained four discrete sets of solutions for each reaction, and we have combined these pairwise to form discrete sets of isospin amplitudes. Some of the solutions were eliminated; first by comparison with data from the channel $\pi^-p\to K_sK_sn$ (the reactions $\pi^+n\to K^-K^+p$ and $\pi^-p\to\bar{K}^0K^0n$ were assumed to satisfy charge symmetry); second, by the requirement that the S waves in $\pi^-p\to K^-K^+n$ and $\pi^+n\to K^-K^+p$ extrapolate to the same value at the pion pole. The solutions eliminated by the second criterion also exhibited unphysical properties in the corresponding isospin amplitudes (i.e., very steep t dependences and considerable mass structure). Of the isospin solutions that passed these criteria, only two showed physically reasonable t dependences in the S and P waves, that is $e^{\approx 12t}$ behavior for the π-exchange waves (the $I=0$ S and $I=1$ P waves), and $e^{\approx 3t}$ behavior for the B-exchange terms (the $I=1$ S and $I=0$ P waves). Selection of the final, unique solution was based on the behavior of the P waves; the accepted solution exhibits phases and moduli close to those expected for the tails of the $\rho(770)$ and $\omega(783)$ resonances.

The only important structures in the final solution occur in the $I=0$ S wave, namely an S^* peak near $\bar{K}K$ threshold, a broad enhancement around 1300 MeV, and a rapid phase advance above 1300 MeV. No significant structure is seen in the $I=1$ S wave for $|t|<0.20$ GeV^2, although we emphasize that our analysis is sensitive only to that part of the $I=1$ S wave which is produced coherently with π exchange (i.e., to the B-exchange part).

Although our experiment is unique in providing a

direct determination of the isospin structure in $(\bar{K}K)^0$, there has been sharp controversy over the isospin of the 1300-MeV enhancement, and we have tried to examine critically the issues raised by other $\bar{K}K$ experiments. Cason *et al.*[3] have argued that the 1300 MeV structure in $\pi^- p \to K_S K_S n$ is produced with anomalously flat t dependence and have speculated that this enhancement has isospin one (e.g., B-exchange production). We have shown that the charge-symmetric reactions $\pi^- p \to \bar{K}^0 K^0 n$ and $\pi^+ n \to K^- K^+ p$ do indeed exhibit flatter t dependence ($e^{\approx 7t}$) in the S wave than would be expected for pure π exchange. However, this effect is simply due to constructive interference between the $I=0$ and $I=1$ S waves, which increases with t. In the reaction $\pi^- p \to K^- K^+ n$, where this interference enters with opposite sign, the S-wave cross section is observed to fall much more steeply ($e^{\approx 17t}$) than π exchange. The pure $I=0$ S wave from our amplitude analysis has in fact a t dependence quite consistent with π exchange ($e^{\approx 11t}$). Although there is a $\approx 10\%$ decrease in the $I=0$ S-wave slope in going from threshold to the 1300-MeV region, this effect seems too small to warrant speculation about non-π-exchange effects in this wave.

Martin *et al.*[5,16,28] have claimed evidence for an $I=1$ S-wave enhancement at ≈ 1300 MeV in the reaction $\pi^- p \to K^- K^0 p$. There is an inherent ambiguity in this reaction in that the S and P waves can only be distinguished by appeal to SU(3) to obtain the expected magnitude of the $\rho(770)$ tail. Their solution for the S wave has a t dependence similar to that expected for the $\rho(770)$. However, they have attributed this steep t dependence to a dominant Z-exchange production mechanism; if correct, their Z-exchange S wave should also contribute incoherently to the charge-exchange reactions $\pi^- p \to K^- K^+ n$ and $\pi^+ n \to K^- K^+ p$. We have found that inclusion of such a resonance in our analysis, while leading to worse fits, would reduce the $I=0$ S-wave amplitude in our favored solution by $\lesssim 15\%$, but would not affect the $I=0$ S-wave phase or the $I=1$ B-exchange S-wave amplitude. In particular, the latter amplitude, which is statistically better determined in both phase and modulus than the $K^- K^0$ S-wave solution of Martin *et al.*, shows no sign of a resonant structure. In any case, our conclusions on the nature of the $I=0$ S wave would not be significantly changed by the presence of the hypothetical $I=1$ Z-exchange enhancement.

We have tried to interpret the $I=0$ S wave in terms of a $\pi\pi$ and $\bar{K}K$ coupled-channel S matrix. From the behavior of the $\pi\pi \to \bar{K}K$ Argand plot, the pole structure in the coupled-channel K matrix, and in particular the $\pi\pi \to \bar{K}K$ phase, we have deduced the existence of a Breit-Wigner resonance with mass 1425 ± 15 MeV and width 160 ± 30 MeV. The $\pi\pi$ phase shifts of Martin and Pennington[33] and the "unique" $\pi\pi$ amplitudes of Becker *et al.*[34] suggest independently that this $\epsilon(1425)$ state is a large effect in $\pi\pi$ elastic scattering, although better data are needed to confirm the behavior of the elastic phase shift in the region 1350–1500 MeV.

We have estimated the coupling strength of the $\epsilon(1425)$ to the $\pi\pi$ and $\bar{K}K$ channels to lie in the range $0.28 \leq (x_\pi x_K)^{1/2} \leq 0.40$, with a positive sign for the relative couplings. The coupling appears to be consistent with that of an $I=0$ $(\bar{u}u + \bar{d}d)$ quark configuration, assuming the Okubo-Zweig-Iizuka rule. However, the coupling strength cannot be uniquely determined without a specific prescription for the S^*-related background intensity. We have shown that the S^* itself does not behave like a narrow Breit-Wigner resonance, and consequently prescriptions for the S^* intensity are not well constrained. By comparison of the $\pi\pi$ and $\bar{K}K$ phase shifts, we have shown that the S^* is best described as a virtual bound state of the $\bar{K}K$ system. As such, the S^* may be expected to produce a large background that falls slowly with mass; *via* unitarity this background causes the $\epsilon(1425)$ peak to shift down to ≈ 1300 MeV and causes substantial broadening of this enhancement.

We have speculated that the $\epsilon(1425)$ is closely related to the $\kappa(\approx 1500)$ (Ref. 9) found in the $K\pi$ S wave, owing to the similarity between the $\pi\pi$ phase shifts predicted from our analysis and the measured $K\pi$ phase shifts. This suggests the existence of a nonet of quark-antiquark scalar mesons, although the $I=1$ and hidden strangeness states remain to be identified in the 1300–1600 MeV mass range. The backgrounds, namely the S^* effect and the strong $\pi\pi$ amplitude in the $\rho(770)$ region, and the analogous background in the $K\pi$ S wave below 1300 MeV, could plausibly be regarded as four-quark states as suggested by Jaffe and Low.[10,11]

ACKNOWLEDGMENTS

We acknowledge helpful communications with A. D. Martin, P. Estabrooks, and E. L. Berger. This work was supported by the U. S. Department of Energy.

APPENDIX

This appendix summarizes the unitarity constraints on the addition of Breit-Wigner and background amplitudes, and shows the precise connection between K-matrix and T-matrix poles. To establish conventions, we define the usual two-channel S and T matrices:

$$\underline{S}(\eta, \delta_1, \delta_2) = \begin{bmatrix} \eta e^{2i\delta_1} & i(1-\eta^2)^{1/2} e^{i(\delta_1 + \delta_2)} \\ i(1-\eta^2)^{1/2} e^{i(\delta_1 + \delta_2)} & \eta e^{2i\delta_2} \end{bmatrix}, \tag{A1}$$

$$\underline{S}(\eta, \delta_1, \delta_2) = \underline{1} + 2i\underline{T} . \quad \text{(A2)}$$

The S matrix satisfies the unitarity constraints

$$\underline{S} \cdot \underline{S}^* = 1 . \quad \text{(A3)}$$

We define the real, symmetric K matrix by the relation

$$\underline{T}^{-1} = \underline{K}^{-1} - \underline{i}, \quad \text{(A4)}$$

where the K matrix has the usual threshold behavior

$$K_{ij} = \left(\frac{q_i q_j}{M^2}\right)^{1/2} \hat{K}_{ij}, \quad \text{(A5)}$$

$\hat{\underline{K}}$ being the reduced K matrix.

There is a simple connection between a K-matrix pole and T-matrix Breit-Wigner behavior. Writing $\underline{K}$ as a sum of background plus pole,

$$K_{ij} = K^B_{ij} + \frac{\gamma_i \gamma_j}{M_0 - M} , \quad \text{(A6)}$$

we obtain a T matrix with the form

$$T_{ij} = T^B_{ij} + \frac{h_i h_j}{M_R - M - i\Gamma/2} . \quad \text{(A7)}$$

Note that the parameters in Eq. (A6) are real, while $\underline{T}^B$ and h_i in Eq. (A7) are complex. Denoting $\underline{\gamma}$ and $\underline{h}$ as the column vectors made up of γ_i and h_i, respectively, the elements in Eqs. (A6) and (A7) are related as follows:

$$(\underline{T}^B)^{-1} = (\underline{K}^B)^{-1} - \underline{i}, \quad \text{(A8a)}$$

$$\underline{h} = (\underline{1} + i\underline{T}^B) \cdot \underline{\gamma}, \quad \text{(A8b)}$$

$$M_R = M_0 + \mathrm{Im}(\underline{h} \cdot \underline{\gamma}), \quad \text{(A8c)}$$

$$\Gamma/2 = \sum \Gamma_i/2 = \mathrm{Re}(\underline{h} \cdot \underline{\gamma}), \quad \text{(A8d)}$$

$$\Gamma_i/2 = |h_i|^2 . \quad \text{(A8e)}$$

Equations (A6)–(A8) generalize to any number of channels. Note that the complex Breit-Wigner couplings h_i are related to the K-matrix residues γ_i by the matrix $\underline{1} + i\underline{T}^B$ [Eq. (A8b)].[40] Thus, for zero background we recover the usual relation $h_i = \gamma_i$. However, if $\underline{T}^B$ is large and varies with mass, then we cannot consistently choose γ_i to be slowly varying functions of mass and also obtain Breit-Wigner couplings $|h_i|$ which are well behaved. Similarly [Eq. (A8c)], M_R and M_0 cannot in general both be regarded as constants. To pick an extreme case, if $\underline{T}^B \to i\underline{1}$ (maximal background), then we would have to allow $\gamma_i \to \infty$ in order to obtain nonzero Breit-Wigner widths in Eq. (A8b). Thus, in order to ensure smoothly behaved Breit-Wigner parameters, it appears easiest to work directly with the representation of Eq. (A7).

The decomposition of Eq. (A7) is somewhat arbitrary, and the relations between resonance and background of Eqs. (A8) depend on the requirement that $\underline{T}^B$ itself is taken to be a unitary matrix. Moreover, if the K matrix were a sum of two poles (i.e., if the background were resonant), the Breit-Wigner properties of the T-matrix resonances would depend on which one was designated as background; interchanging the two poles would result in different mass and width parameters, not just an interchange of the resonances, in Eq. (A7). However, consideration of practical cases shows that the differences would in fact be slight, and the requirement of smooth Breit-Wigner parameters would naturally lead to a unique decomposition in Eq. (A7). See Ref. 41 for further discussion.

Since the K matrix is not known *a priori*, it is useful to eliminate the parameters γ_i and M_0 from Eqs. (A8); using Eqs. (A2), (A3), and (A8b) we obtain[42]

$$\underline{h} = \underline{S}^B \cdot \underline{h}^* , \quad \text{(A9)}$$

where $\underline{S}^B(\eta_B, \delta^B_1, \delta^B_2)$ is the S matrix corresponding to $\underline{T}^B$. The solutions to the two complex equations implied by Eq. (A9) have the form[41]

$$h_i = e^{i\theta_i + \delta^B_i} (\Gamma_i/2)^{1/2}, \quad \text{(A10)}$$

where the unitarity phases θ_i are given by

$$\cos 2\theta_i = \frac{2x_i - 1 + \eta_B{}^2}{2x_i \eta_B} . \quad \text{(A11)}$$

In Eqs. (A10) and (A11), $x_i = \Gamma_i/\Gamma$ are the resonance branching ratios, and η_B, δ^B_1, and δ^B_2 are the background elasticity and phase shifts. A further constraint on the unitarity angles which follows from Eq. (A9) is

$$\sin^2(\theta_1 + \theta_2) = \frac{1 - \eta_B{}^2}{4 x_1 x_2} . \quad \text{(A12)}$$

Equation (A12) admits two solutions; the first solution, denoted (+), can be chosen with $\theta_1 + \theta_2$ in the first quadrant; the second (–) solution is the complement of the (+) solution, $\pi - \theta_1 - \theta_2$, and lies in the second quadrant. These solutions correspond to the signs of the pairs $(\sin 2\theta_1, \sin 2\theta_2)$, which are unspecified by Eq. (A11); the (+) solution corresponds to the (+, +) sign pairing, and the (–) to the (–, –) pairing. There are thus two and only two discrete solutions for the unitarity phases θ_i, characterized by $\theta_1 + \theta_2$ being in the first (+) or second (–) quadrants.

Given the background parameters η_B, δ^B_1, and δ^B_2 and the Breit-Wigner parameters M_R, Γ_1, and Γ_2, we can reconstruct the two discrete solutions for the T matrix in Eq. (A7) corresponding to the (+) and (–) unitarity phases. Our most useful result concerns the cross-channel amplitude T_{12}. Denot-

ing the Breit-Wigner contribution to Eq. (A7) by $\underline{T}^R$, that is,

$$T_{12} = T_{12}^B + T_{12}^R , \tag{A13}$$

we obtain, after some algebra, the relations

$$T_{12} = (x_1 x_2)^{1/2} \left| \sin(\delta^R + \theta_1 + \theta_2) \right| e^{i(\delta^R + \delta_1^B + \delta_2^B)} , \tag{A14a}$$

$$T_{12}^B = (x_1 x_2)^{1/2} \sin(\theta_1 + \theta_2)\, e^{i(\delta_1^B + \delta_2^B)} , \tag{A14b}$$

$$T_{12}^R = (x_1 x_2)^{1/2} \sin\delta^R\, e^{i\delta^R + \delta_1^B + \delta_2^B + \theta_1 + \theta_2} , \tag{A14c}$$

where

$$\delta^R = \mathrm{Arg}(M_R - M + i\Gamma/2) . \tag{A14d}$$

The amplitudes T_{12}, T_{12}^B, and T_{12}^R form three sides of a triangle in the complex plane, as depicted in Fig. 32. The most crucial unitarity constraint is contained in the statement

$$\mathrm{Arg}(T_{12}) = \mathrm{Arg}(T_{12}^B) + \delta^R \tag{A15}$$

which follows from Eqs. (A14a) and (A14b). This constraint fixes the angle between T_{12} and T_{12}^B in Fig. 32, and illustrates the origin of the two discrete solutions to the unitarity phases. Given the magnitude of T_{12}^R from the Breit-Wigner parameters, there are precisely two ways to close the triangle in Fig. 32, and these correspond to the two solutions $\theta_1 + \theta_2$ and $\pi - \theta_1 - \theta_2$ for the unitarity phases discussed above.

The relations given in Eq. (A14) can be derived algebraically from Eqs. (A7) and (A9)–(A12), and they can also be read off from the geometry of Fig. 32, given the constraint of Eq. (A15). The latter constraint is, in fact, quite general. In a multichannel case, the corresponding constraint would be[43]

$$\mathrm{Det}(\underline{S}) = \exp\left[2i\left(\sum_i \delta_i^B + \delta^R\right)\right] . \tag{A16}$$

In the two-channel case, $\mathrm{Det}(\underline{S})$ happens to be closely related to $\mathrm{Arg}(T_{12})$ [cf. Eq. (A1)]. Equations (A14), though not intuitively obvious, exhibit sensible behavior in the limiting cases: (a) for $T^B \to 0$ we obtain $T_{12} \to T_{12}^R$; (b) for $\delta^R \to 0$ (far from resonance), we get $T_{12} \to T_{12}^B$. In the limit $T_{12}^B \to O(\eta_B \to 1, \delta_1^B, \delta_2^B \to 0)$, we obtain $\theta_1 + \theta_2 \to 0\ (\pi)$ for the + (−) solutions and $T_{\pm}^R \to \pm(x_1 x_2)^{1/2} e^{i\delta^R}$ ($T^R \to -(x_1 x_2)^{1/2} e^{i\delta^R}$). Thus we may identify these solutions as having, respectively, positive and negative relative couplings of the resonance to channels 1 and 2. Two important unitarity constraints follow from Eqs. (A14a) and (A14b), namely,

$$|T_{12}| \leq (x_1 x_2)^{1/2} , \tag{A17a}$$

$$|T_{12}^B| \leq (x_1 x_2)^{1/2} . \tag{A17b}$$

The amplitudes T_{11} and T_{22} can be constructed from Eq. (A7). In practice, for the case of interest in which $x_1 \gg x_2$, it is a reasonable approximation to write

$$(h_1)^2 \approx e^{2i\delta_1^B} \Gamma_1/2 , \tag{A18a}$$

$$(h_2)^2 \approx 0 \tag{A18b}$$

and as a result

$$\delta_1 \approx \delta_1^B + \delta^R , \tag{A19a}$$

$$\delta_2 \approx \delta_2^B . \tag{A19b}$$

Equations (A19a) and (A19b) hold to within ~10° for the domain $x_1 > 0.8$ ($x_2 < 0.2$). Note that the relation

$$\delta_1 + \delta_2 = \delta_1^B + \delta_2^B + \delta^R \tag{A20}$$

is still exact, and is identical with Eq. (A15).

One difficulty in the above formalism is that the partial widths Γ_i cannot be chosen independent of the background. For example, the unitarity constraint of Eq. (A17b), which implies a minimum coupling for $(x_1 x_2)^{1/2}$, could in principle conflict with other dynamical requirements such as SU(3) symmetry or the OZI rule. Novoseller[38] has suggested, in effect, a redefinition of the resonance couplings that decouples these parameters from the background. The new couplings g_i are obtained from a unitary transformation on the h_i couplings,

$$\underline{g} = (\underline{S}^{B*})^{1/2} \cdot \underline{h} , \tag{A21}$$

which preserves the total width

$$\Gamma/2 = \sum_i g_i^2 = \sum_i |h_i|^2 . \tag{A22}$$

The parameters g_i are real [this follows from Eq. (A9)]. That the partial widths, $\Gamma_i'/2 = g_i^2$, are independent of the background can be seen from substitution for h_i in Eq. (A7):

$$\underline{S} = (\underline{S}^B)^{1/2} \cdot \left[\underline{1} + \frac{2i\underline{g}\underline{g}}{M_R - M - i\Gamma/2}\right] \cdot (\underline{S}^B)^{1/2} . \tag{A23}$$

Because $\underline{S}$ is manifestly unitary, the g_i can be chosen independent of unitarity constraints. In practice, the partial widths Γ_i' can be determined once a solution is found for $\underline{S}_B$ and $\underline{h}$.

---

*Present address: University of Miami, School of Medicine, P.O. Box 520875 Biscayne Annex, Miami, Florida 33152.

†Present address: P.O. Box 878, Woodland Park, Colorado 80863.

[1] A. J. Pawlicki *et al.*, Phys. Rev. D 15, 3196 (1977).

[2] H. J. Lipkin, Phys. Rev. 176, 1709 (1968).

[3] N. M. Cason *et al.*, Phys. Rev. Lett. 36, 1485 (1976);

V. A. Polychronakos *et al.*, Phys. Rev. D 19, 1317 (1979).
[4]W. Wetzel *et al.*, Nucl. Phys. B115, 208 (1976).
[5]A. D. Martin *et al.*, Phys. Lett. 74B, 417 (1978).
[6]A. J. Pawlicki *et al.*, Phys. Rev. Lett. 37, 1666 (1976).
[7]D. Cohen, in *Proceedings of the Fifth International Conference on Experimental Meson Spectroscopy*, edited by E. von Goeler and R. Weinstein (Northeastern University Press, Boston, 1977), p. 238.
[8]D. Morgan, in *New Directions in Hadron Spectroscopy*, proceedings of the Summer Symposium, Argonne, Illinois, 1975, edited by S. L. Kramer and E. L. Berger (Argonne National Laboratory, Argonne, 1975), p. 45; Phys. Lett. 51B, 71 (1974).
[9]P. Estabrooks, Phys. Rev. D 19, 2678 (1979).
[10]R. L. Jaffe, Phys. Rev. D 15, 267 (1977).
[11]R. L. Jaffe and F. E. Low, Phys. Rev. D 19, 2105 (1979).
[12]A. B. Wicklund *et al.*, Phys. Rev. D 17, 1197 (1978).
[13]A. D. Martin and C. Michael, Nucl. Phys. B84, 83 (1975).
[14]G. Grayer *et al.*, Nucl. Phys. B75, 189 (1974).
[15]P. Estabrooks *et al.*, in π-π *Scattering—1973*, proceedings of the International Conference on π-π Scattering and Associated Topics, Tallahassee, 1973, edited by P. K. Williams and V. Hagopian (AIP, New York, 1973), p. 37.
[16]A. D. Martin and E. N. Ozmutlu, Nucl. Phys. B158, 520 (1979).
[17]E. Barrelet, Nuovo Cimento 8A, 331 (1972).
[18]A. J. Pawlicki *et al.*, Phys. Rev. Lett. 37, 971 (1976). We have used the same D-wave phase for reactions (1) and (2); for $|t|<0.08$ GeV^2 the A_2 amplitude is ignorable.
[19]Since the absolute normalization is not given for the data in Ref. 3, we have normalized them to give $\langle \sigma Y_4^0 \rangle$ equal to that for reaction (2) in the f-mass region. Note that this procedure automatically corrects for the unobserved K_LK_L final state.
[20]W. Fickinger, private communication.
[21]M. J. Corden *et al.*, Nucl. Phys. B138, 235 (1978).
[22]M. J. Emms *et al.*, Phys. Lett. 58B, 117 (1975).
[23]M. H. Shaevitz *et al.*, Phys. Rev. Lett. 36, 8 (1976).
[24]M. J. Emms *et al.*, Nucl. Phys. B98, 1 (1975).
[25]We have parametrized $P_{I=1}$ as follows:

$$P_{I=1}=\frac{1}{p_{\rm lab}}\frac{C\sqrt{-t}}{\mu^2-t}e^{B_P(t-\mu^2)}\left(\frac{3M^2}{q_\pi}\right)^{1/2}\times\frac{M_0(\Gamma_\pi\Gamma_K)^{1/2}}{M_0^2-M^2-iM_0(\Gamma_\pi+2\Gamma_K)},$$

where

$$\Gamma_\pi=\Gamma_\rho\left(\frac{q_\pi}{q_\rho}\right)^3\frac{M_0}{M}\frac{(1+R^2q_0^2)}{(1+R^2q_\pi^2)}$$

and

$$\Gamma_K=\frac{\Gamma_\rho}{4}\left(\frac{q_K}{q_\rho}\right)^3\frac{M_0}{M}\frac{(1+R^2q_0^2)}{(1+R^2q_K^2)}.$$

Here q_π and q_K refer to the $(\pi^-\pi^+)$ and (K^-K^+) center-of-mass momenta, respectively; q_0 is q_π at the ρ^0 mass, which is denoted by M_0. R is taken to be 3.5 GeV^{-1}, $\Gamma_\rho=150$ MeV, $M_0=773$ MeV. The OPEA parameters, taken from Ref. 12, are $C=3.2$ mb$^{1/2}$ and $B_P=3.0$ GeV^{-2}. The factor of $\frac{1}{4}$ in Γ_K comes from SU(3), while the expression $\Gamma_\pi+2\Gamma_K$ in the Breit-Wigner denominator allows for the $\overline{K}^0K^0$ contribution to $\Gamma_{\rm tot}$.
[26]A. C. Irving, Phys. Lett. 70B, 217 (1977).
[27]D. J. Crennell *et al.*, Phys. Rev. Lett. 27, 1674 (1971).
[28]A. D. Martin *et al.*, Nucl. Phys. B140, 158 (1978).
[29]A. C. Irving, Nucl. Phys. B105, 491 (1976).
[30]By "Breit-Wigner" poles we mean companion T-matrix poles on sheets II and III. See Ref. 8.
[31]B. Hyams *et al.*, Nucl. Phys. B100, 205 (1975).
[32]P. Estabrooks and A. D. Martin, Nucl. Phys. B95, 322 (1975).
[33]A. D. Martin and M. R. Pennington, Ann. Phys. (N.Y.) 114, 1 (1978).
[34]H. Becker *et al.*, Nucl. Phys. B151, 46 (1979).
[35]To obtain the phase shifts in Fig. 29(a), we averaged the phases of the g_s and h_s amplitudes of Ref. 34 and referenced these against the D-wave Breit-Wigner phase, using the $f(1270)$ parameters of Ref. 34. Corrections were made for the $I=2$ contributions, as in Ref. 32.
[36]The phase $\phi(\pi\pi\to\overline{K}K)$ from solution I(b) is not well determined close to $\overline{K}K$ threshold owing to the smallness of the reference D wave. The phases shown in Figs. 26 and 29 in effect use the P waves as well as the D waves as overall phase references, and this allows a much better determination of $\phi(\pi\pi\to\overline{K}K)$ near threshold. We have checked the behavior of the moments near threshold for consistency with these phases. We note that $\phi(\pi\pi\to\overline{K}K)=\delta_\pi+\delta_K$ must approach $\approx 180°$ at $\overline{K}K$ threshold, where $\delta_\pi\simeq 180°$ and $\delta_K=0°$.
[37]S. D. Protopopescu *et al.*, Phys. Rev. D 7, 1279 (1973); G. Grayer *et al.*, in π-π *Scattering—1973*, proceedings of the International Conference on π-π Scattering and Associated Topics, Tallahassee, 1973, edited by P. K. Williams and V. Hagopian (AIP, New York, 1973), p. 117.
[38]D. E. Novoseller, Nucl. Phys. B (to be published).
[39]P. Estabrooks *et al.*, Nucl. Phys. B133, 490 (1978).
[40]The matrix $\underline{1}+i\underline{T}^B$ is equivalent to $(\underline{1}-i\underline{K}^B)^{-1}$ and to $\frac{1}{2}(\underline{1}+\underline{S}^B)$.
[41]P. W. Coulter, Phys. Rev. Lett. 29, 450 (1972); Phys. Rev. D 7, 7 (1973).
[42]C. J. Goebel and K. W. McVoy, Phys. Rev. 169, 1932 (1967).
[43]R. H. Dalitz and R. G. Moorhouse, Proc. R. Soc. London A318, 279 (1970).